Structural complexities and tectonic barriers controlling recent seismic activity ~~of~~ in the Pollino area (Calabria-Lucania, Southern Italy) - constraints from stress inversion and 3D fault model building.

Daniele Cirillo[1-2]*, Cristina Totaro[2-3], Giusy Lavecchia[1-2], Barbara Orecchio[2-3], Rita de Nardis[1-2], Debora Presti[2-3], Federica Ferrarini[1-2], Simone Bello[1-2] and Francesco Brozzetti[1-2]*

[1] Università degli studi "G. d'Annunzio" Chieti-Pescara, DiSPUTer, via dei Vestini 31, 66100 Chieti, Italy.
[2] CRUST Centro inteRUniversitario per l'analisi SismoTettonica tridimensionale, Italy.
[3] Università degli studi di Messina, Dipartimento di Scienze Matematiche e Informatiche, Scienze Fisiche e Scienze della Terra -Viale F. Stagno D'Alcontres, 98166, Messina, Italy

Correspondence to: Daniele Cirillo (daniele.cirillo@unich.it) and Francesco Brozzetti (francesco.brozzetti@unich.it)

Abstract. We reconstruct the 3D Fault Model of the structures causative of the ~~faults which released the~~ 2010-2014 Pollino seismic ~~sequence~~activity by ~~The integration~~integrating ~~of field geology~~structural-geological and high-resolution seismological data~~. allowed us to reconstruct the 3D Fault Model of the sources which gave rise to the 2010-2014 Pollino seismic sequence~~. ~~The model is~~ We constrained the model at the surface ~~by structural geological data~~with fault-slip data and ~~which provide the true attitude of the single faults and their cross cut relationships. A~~at depth, ~~the fault geometry was obtained~~by~~ using the distributions of selected high-quality relocated hypocenters. Relocations were ~~were carried out~~performed through ~~a~~the non-linear Bayloc algorithm, followed by the double-difference relative location method HypoDD~~,~~ applied to a 3D P-wave velocity model.

Geological and seismological data ~~converge in describ~~highlighting an asymmetric active extensional fault system characterized by an E to NNE-dipping low-angle detachment, with ~~with its~~high-angle synthetic splays, and SW- to WSW-dipping, high-angle antithetic faults.

~~The c~~Clusters of hypocenters ~~Hypocenter clustering~~ and the ~~peculiar~~ time-space evolution of the seismic~~ity~~ ~~activity~~ ~~highlight~~suggest that two sub-parallel WSW-dipping seismogenic sources~~, namely the~~(*i.e.,* the Rotonda-Campotenese and Morano-Piano di Ruggio faults~~)~~, ~~were~~are responsible of the ~~activated during the~~ 2010-2014 ~~seismic crisis~~sequence~~activity~~. T~~The size~~area of the ~~activated~~seismogenic patches, ~~reconstructed by~~obtained projecting the hypocenters of the early aftershocks on the 3D ~~seismogenic~~fault planes, are consistent with the observed magnitude of the ~~associate~~strongest events ($M_{w=}$5.2, and $M_{w=}$4.3).

~~By applying~~Since ~~to the activated structures the appropriate~~ earthquake-scaling relationships~~, based on fault length and fault area, we infer that the maximum expected magnitudes calculated using the fault area are the more reliable. W~~we

33 estimatedprovide maximum expected magnitudes of M$_w$=6.4 for the Rotonda-Campotenese and M$_w$=6.2 for the Morano-Piano

34 di Ruggio faults, we may supposededucededucing that, during the sequence, the both thethe two structures faults did not release

35 entirely their maximum seismic potential during the 2010-2014 seismic sequence, with clear implication for seismic hazard

36 evaluations.

37 The reconstructed 3D fault model also points out the relationships between the activated fault system

38 The size of the activated patches, reconstructed by projecting on the 3D seismogenic fault planes the early aftershocks of the

39 seismicity clusters, are consistent with the observed magnitude of the associate strongest events.

40 Finally, wWe point out that and the western segment of the Pollino Fault. This latter, despite not being presently active was

41 not involved in the recent seismic activity, acts as but could have acted as a barrier to the southern propagation of the Rotonda-

42 Campotenese and Morano Piano di Ruggioseismogenic faults, limiting their dimensions and seismogenic potentialthe

43 magnitude of the generated earthquakes.

44 **1 Introduction**

45 In recent years, the reconstruction of 3D Fault Models (hereinafter referred to as 3DFM) of potentially seismogenic structures,

46 obtained by integrating surface ad subsurface data, has become an increasingly practiced methodology in thefor seismotectonic

47 analysis studies of regions undergoing active deformation (*e.g.*, SCEC, 2021; Lavecchia et al., 2017; Castaldo et al., 2018;

48 Klin et al., 2019; Di Bucci et al., 2021; SCEC, 2021;). The techniques to obtain the 3DFM integrate all the available surface

49 ad subsurface data and allow to reconstruct the 3D geometry of seismogenic structures. In particular, dDetailed structural-

50 geological data are used to define the active faults geometry of the active faults at the surface whereas high-quality geophysical

51 data are needed to constrain the shape of the sources at depth. If these conditions are met, The 3DFM reconstruction building

52 helps allows determining the spatial relationships and the interactions between adjacent sources and identifying any barriers

53 hampering at depth the propagation of the coseismic rupture. Moreover, such an approach leads to accurately estimate

54 estimating with great accuracy the area of the seismogenic fault, and therefore the associated expected magnitude.

55

56 In Italy, reconstruction of 3DFM could give important achievements in the Apennine active extensional belt which is affected

57 by significant seismic activity (ISIDe, 2007; Rovida et al., 2020). This belt consists of ~NW-SE striking Quaternary normal

58 fault systems, and the related basins, located just west or within the culmination zone of the chain (Calamita et al., 1992;

59 Brozzetti and Lavecchia, 1994; Lavecchia et al., 1994, 2021; Barchi et al., 1998; Cinque et al., 2000; Brozzetti, 2011; Ferrarini

60 et al., 2015, 2021). Its structural setting is very complicated due to a polyphase tectonic history characterized by the

61 superposition of Quaternary post-orogenic extension on Miocene-Early Pliocene folds and thrusts and on Jurassic-Cretaceous

62 sin-sedimentary faults (*e.g.*, Elter et al., 1975; Ghisetti and Vezzani, 1982, 1983; Lipmann-Provansal, 1987; Mostardini and

63 Merlini, 1986; Patacca and Scandone, 2007; Mostardini and Merlini, 1986; Vezzani et al., 2010,; Ferrarini et al., 2017;

64 Brozzetti et al 2021 among others).

65

~~Since the beginning of the Pleistocene, regional normal fault systems dissected the contractional structures with displacements that locally reach some km.~~ Over time, detailed structural geological studies made it possible to recognize several seismogenic faults in the Apennine active extensional belt (Barchi et al., 1999; Galadini and Galli, 2000; Maschio et al., 2005; Brozzetti, 2011) and, in some cases, to document, through paleo-seismological data, their ~~timing of~~ reactivation during the Holocene (Galli et al., 2020). Furthermore, the increasing availability of high-resolution~~in recent years, new technologies~~ imagery have ~~made it possible~~allows ~~to reconstruct~~ fault ~~patterns~~ mapping at the sub-meter scale ~~with very high precision, thus allowing to constrain the fault structures at the surface at sub-meter scale resolution~~ (e.g., Westoby et al., 2012; Johnson et al., 2014; Cirillo, 2020; Bello et al., 2021b, 2021c)~~.), Finally,~~while ~~A~~accurate geophysical prospections (e.g., ~~G~~ground ~~Penetration~~ Penetrating Radar), ~~aimed at the study of historical earthquakes' surface faulting,~~ allow~~ed to investigate~~ investigating the ~~sub-fault~~ surface at shallow depths (few ~~tens of~~meters or tens of meters; (e.g., Gafarov et al., 2018; Ercoli et al., 2013, 2021)~~., but high-resolution only providing constraints at shallow depths (few tens of m).~~

Conversely, the geometries of the faults at ~~greater~~ depths are ~~poorly reliable~~rarely available~~er~~ since high-resolution deep geological and geophysical constraints are often lacking (i.e., deep wells and/or seismic profiles).

In fact, in the last decades, seismic reflection prospecting and deep-well exploitation for hydrocarbon research, avoided the area affected by active extension, and focused on the eastern front of the chain and on the Adriatic-Bradanic foreland basin system (ViDEPI:www.videpi.com, last access: 19 april 2021). ~~(ViDEPI: www.videpi.com).~~

~~The absence of the latter~~This lack can be compensated with well relocat~~l~~ized high-resolution seismological datasets, ~~and integrating them~~to be integrated with geological ones. In Italy, datasets of ~~provides a new opportunity to image the three-dimensional shape of the sources~~The availability of high-resolution seismological datasets, to be integrated with geological ones, provides a new opportunity to image the tri-dimensional shape of the sources.

~~Datasets characterized by h~~h~~H~~ighly precise re-~~locations~~located ~~of~~hypocenters were collected during recent seismic sequences ~~associated with~~ low/medium- and high-magnitude earthquakes (Chiaraluce et al., 2004, 2005, 2011, 2017; Totaro et al., 2013, 2015). These sequences include thousand~~s~~ of earthquakes~~—~~ (in confined ~~rock~~ volumes of rock) which appear to roughly connect with the fault traces ~~mapped~~at the surface. Therefore, such distributions of earthquakes are generally referred to as ongoing rupture processes affecting an entire, or wide portion~~s~~ of~~,~~ the seismogenic faults.

In some cases, ~~(Chiaraluce et al., 2017; Valoroso et al., 2017)~~ very high-resolution hypocenter locations (Chiaraluce et al., 2017; Valoroso et al., 2017), as well as reflection seismic lines, allow to clearly highlight the seismogenic structures at depth (Lavecchia et al., 2011, 2012a, 2012b, 2015, 2016).

~~A number of favourable factors make the Calabria-Lucania boundary (southern Apennines) an interesting study area for the reconstruction of 3DFM, using good quality seismological data.~~

~~This~~The study area of this work includes the northern sector of the so-called "Pollino seismic gap" (Fig. 1), in which paleo-earthquakes up to M=7 are documented (Michetti et al., 1997; Cinti et al., 1997, 2002) whereas the location and size of

3

98 seismogenic sources are a matter of debate (Michetti et al., 2000; Cinti et al., 2002; Papanikolaou and Roberts, 2007; Brozzetti

99 et al., 2009, 2017a). In the sector,

100 ~~Recently, using structural geological and morpho-structural survey techniques,~~ Brozzetti et al. (2017a) mapped a set of active

101 faults between the Mercure, Campotenese, and Morano Calabro Quaternary basins (Fig. 1a).

102 During the 2010-2014 -time interval, this area was affected by a low to moderate instrumental seismicity (Pollino seismic

103 ~~sequence~~activity), climaxing ~~at~~ with the 25 October 2012, M_w 5.2 Mormanno earthquake, ~~with~~ and characterized by thousands

104 of recorded events (Totaro et al., 2013, 2015). During the sequence, two other~~s~~ moderate ~~strongest~~ event~~s~~ occurred close to

105 the village of Morano Calabro: ~~the~~ on 28 May 2012 (M_w 4.3), and ~~the~~ on 6 June 2014 (M_w 4.0~~) earthquakes (~~; Fig. 1b).

106 According to Brozzetti et al. (2017a),

107 ~~T~~the whole seismicity was arranged in two major clusters and a minor one ~~(Totaro et al., 2015)~~. Each major cluster was

108 associated with one ~~strong~~ moderate event~~s~~ and was generated by an independent seismogenic structure ~~(Brozzetti et al.,~~

109 ~~2017a)~~.

110 The pre-existence of a seismic network, that was implemented after the ~~start~~ beginning of the sequence.~~, made it possible to~~

111 ~~increase the precision of the hypocentral determination and to relocate the events after an accurate selection, providing~~

112 provided a high-quality database of relocated hypocenters (Totaro et al., 2013, 2015; Brozzetti et al., 2017a).

113

114 In such context we~~, the main purposes of this work are to:~~

115   reconstruct the 3DFM ~~activated~~ involved by the ~~Pollino~~ 2010-2014 seismic ~~sequence;~~activity

116 to investigate, at depth, the ~~possible interactions between the various seismogenic sources, determining that is the~~ cross-cut

117 relationships between the faults having different ~~strikes, dip angles~~ attitudes~~,~~ and timing of activation. Furthermore, we~~;~~

118 provide the geometric parameters of the sources ~~aimed at~~ to estimat~~eing~~ the ~~maximum~~ expected magnitudes ~~based on the~~

119 ~~defined 3D source~~.

120 ~~Finally, we~~We also~~Finally, we~~ discuss some 3D-seismotectonics methodological aspects ~~which are of general interest for~~

121 ~~researchers approaching three dimensional seismotectonics in any structural context. These aspects~~ which dwell on the

122 improvements that the proposed procedure provides to the definition of the source model~~,~~ and on ~~the~~ its limits. ~~of the method~~

123 ~~imposed by the type and quality of the available data, and the possible causes of errors with the relative ranges of variation.~~
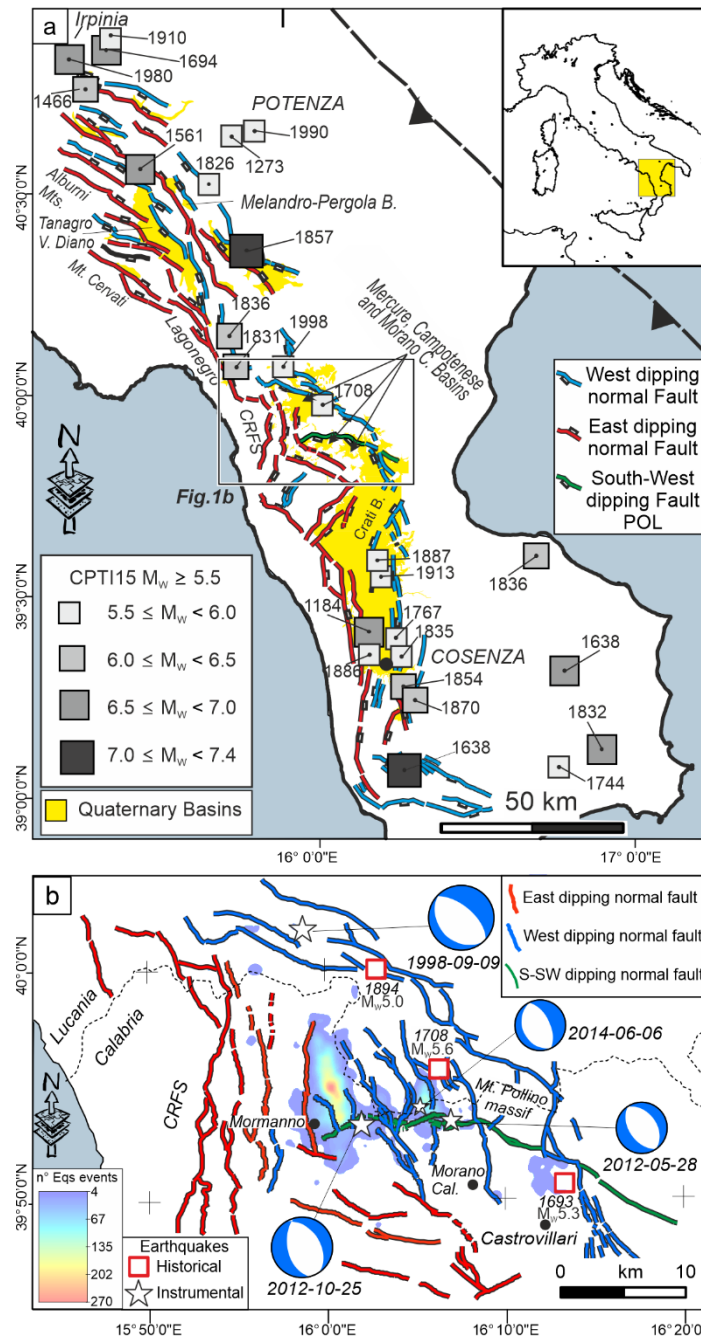
Figure 1: Seismotectonic context of the study area. (a) Active faults of the Southern Apennines with major historical and instrumental earthquakes from Parametric Catalogue of Italian Earthquakes, CPTI15 v3.0 (Rovida et al., 2020, 2021). (b) Normal faults cropping out between the Mercure, Campotenese, Morano Calabro, and Castrovillari Quaternary basins (after Brozzetti et al., 2017a) andwith Distribution distribution of the 2010-2014 Pollino seismic sequence activity (contoured areas) withand focal mechanisms are theof the (events with Mw>4.0; ((Totaro et al., 2015, 2016). Normal faults between the Mercure, Campotenese, Morano Calabro and Castrovillari Quaternary basins are reported (after Brozzetti et al., 2017a).

5

131

2. ~~.1~~ Geological Setting

The Mt. Pollino massif is located at the Calabrian-Lucanian boundary (Fig. 1) in a sector of the Apennines structured during the Middle-Late Miocene contractional tectonics which ~~that~~ affected the western Adria Plate (D'Argenio, 1992; Patacca and Scandone, 2007; Ietto and Barilaro, 1993; Iannace et al. 2004, 2005, 2007).

The surface geology in this area is characterized by the superposition of two main tectonic units ~~each~~ derive~~d~~s from different paleogeographic domains. These are represented~~,~~ (from bottom to top), by 1) ~~:~~

~~—~~the "Apenninic" units (or "Panormide~~"~~; Triassic - Early Miocene~~"~~), which are characterized by carbonate platform, including the Verbicaro and Pollino Units ~~with an age from Triassic to Early Miocene~~, locally intruded by basaltic rocks (Ogniben, 1969, 1973; Amodio-Morelli et al., 1976; Iannace et al., 2007; Patacca and Scandone, 2007; Vezzani et al., 2010; Tangari et al., 2018)~~;~~

~~and, 2) by —~~the "Ligurian" units (Late Jurassic – Early Cretaceous), that consist of ophiolites and deep-sea sedimentary deposits derived from the Western Tethys oceanic basin (Ogniben, 1969, 1973; Amodio-Morelli et al., 1976; Liberi et al., 2006; Liberi and Piluso, 2009; Filice et al., 2015).

During uppermost Miocene and ~~–~~Pliocene times, the folds and thrusts ~~edifice~~ pile was displaced by WNW-ESE-striking left-lateral wrench faults~~, among which, the Pollino fault (POL) played an important role (Fig. 1b)~~ (Grandjacquet~~,~~ 1962; Ghisetti and Vezzani~~,~~ 1982; Van Dijk et al., 2000).

Subsequently, regional-scale extensional fault~~s~~ systems, consisting of E- and W-dipping conjugate normal faults, dissected the Tyrrhenian side and the core of the orogen which assumed a typical basin and range relief.

~~The~~ This Quaternary ~~extensional~~ phase ~~also~~ caused the reactivation of the previous strike-slip structures~~. In particular, the reactivation of~~ such as the Pollino fault (POL), whose ~~of which the with~~ normal to normal-oblique kinematics, has been documented ~~at least~~ since the Early-Middle Pleistocene (Ghisetti and Vezzani, 1982, 1983, Brozzetti et al., 2017a).

At present~~Actually~~, the age of onset of the extensional tectonic is still under discussion; it is referred by some authors to the Early Pleistocene (Ghisetti and Vezzani, 1982; Schiattarella et al., 1994; Papanikolaou and Roberts 2007; Barchi et al., 2007; Amicucci et al., 2008; Brozzetti, 2011; Robustelli et al., 2014), ~~whereas~~ while it would not be older than the Middle Pleistocene, according to others (Caiazzo et al., 1992; Cinque et al. 1993; Hyppolite et al., 1995; Cello et al., 2003; Giano et al., 2003; Spina et al., 2009; Filice and Seeber, 2019).

In the Campania-Lucania and north-Calabria sectors of the southern Apennines, the active extensional belt includes three main alignments of normal faults and Quaternary basins, arranged in a right-lateral en-echelon setting (Fig. 1a). From north to south they are~~: i) northern alignment: including the~~ the internal alignment, including the Irpinia fault, ~~the~~ ~~and the~~ Melandro-Pergola and ~~and~~ Agri basins~~; ii) intermediate, the~~ the intermediate ~~alignment~~one.~~:~~ developing from the Tanagro-Vallo di Diano basins to the Mercure-Campotenese and Morano Calabro basins~~, and iii) southern alignment:than~~the external ~~one~~alignment, developing from the Castrovillari fault to the southern Crati basin (Pantosti and Valensise, 1990, 1993; Ascione et al., 2013; Galli and Peronace, 2014; Ghisetti and Vezzani, 1982, 1983; Barchi et al., 1999, 2007; Blumetti et al., 2002; Amicucci et al., 2008; Maschio et al., 2005; Villani and Pierdominici, 2010; Brozzetti, 201~~1~~1,~~1,~~ Faure Walker et al., 2012; Brozzetti et al., 2009, 2012, 2017a, 2017b; Robustelli et al., 2014; Sgambato et al., 2020; Bello et al., 2021a).

All along the above alignments, the geometry and kinematics of the major normal faults are kinematically compatible with a SW-NE direction of extension (Maschio et al. 2005; Brozzetti, 2011; Brozzetti et al., 2009; 2017a). A similar orientation of the T-Axis is obtained from the focal mechanisms of the major earthquakes from CMT and TDMT databases (Pondrelli et al., 2006; Scognamiglio et al., 2006; Montone ~~et al~~and Mariucci., ~~2012~~2016; Totaro et al., 2016) and from GPS data (D'Agostino et al., 2014)~~.~~ ~~;~~ Cheloni et al. (2017)~~. demonstrated, from geodetic GPS and DInSAR analysis, that the Pollino area was affected by important deformation rates during the 2010-2014 seismic activity, with increasing and decreasing of slip values due to the temporal and spatial behavior of the recorded seismicity (Passarelli et al. 2015).~~ The recent ~~present~~ activity of these normal fault~~s~~ systems is firstly suggested by the control exerted on the distribution of seismicity, as shown by the location of upper crustal instrumental earthquakes (ISIDe ~~database,~~ Working Group, 2007 ~~INGV~~; Brozzetti et al., 2009; Totaro et al., 2014, 2015; Cheloni et al., 2017; Napolitano et al., 2020, 2021; Pastori et al., 2021; Sketsiou et al., 2021) and of destructive historical events (Fig. 1~~,~~; Rovida et al., 2021).

~~The As anticipated, t~~The area affected by the 2010-2014 seismicity extends from the Mercure ~~basin~~ to the Campotenese and Morano Calabro basins ~~that are~~. along the intermediate extensional fault ~~fault~~ alignment ~~described above~~which, according to ~~. In this area, recent structural geological works~~pPrevious literature, consists of ~~highlighted~~ three main sets of genetically-linked normal and normal-oblique active faults (Brozzetti et al., 2017a; Figs 1b, 2; Acronyms list in Supplementary Text 1). The first one, ~~E- to NNE-dipping,~~ referred to as the Coastal Range Fault Set (CRFS; red lines in Figs 1b, 2) dips E- to NNE and encompasses four sub-parallel major fault segments named~~which~~, from west to east, ~~are:~~ Gada-Ciagola (GCG), Papasidero (PPS), Avena (AVN) and Battendiero (BAT)~~faults~~. Their strike ~~direction~~ varies southward from N-S to WNW-ESE.

The other two fault sets strike ~NW-SE~~,~~ and dip ~SW (blue lines in Figs 1b, 2). The western one, developing from Rotonda to Campotenese villages ~~through the 2010-2014 seismic sequence epicentral area~~, consists of two main right-stepping en-echelon ~~fault~~ segments. They are referred to as ROCS system~~,~~ and include the Rotonda-Sambucoso (RSB) and Fosso della Valle-Campotenese (VCT; Fig.~~1b~~ 2). The eastern set, including the en-echelon Castello Seluci - Piana Perretti - Timpa della Manca (~~CPST~~CSPT), the Viggianello-~~Piano~~ Piani di ~~del~~ Pollino (VPP) and the Castrovillari (CAS) faults, represents the break-away zone of the Quaternary extensional belt. In the area between these two W-dipping sets, the W to NW-dipping Morano

198 Calabro-Piano di Ruggio (MPR) and Gaudolino (GDN) faults, show ~~evidences~~evidence of Late Quaternary activity (Brozzetti

199 et al., 2017a; Fig. ~~1b~~2).

200 ~~Geodetic~~ GPS and DInSAR analysis demonstrated ~~that~~as the Pollino area was affected by important deformation rates during

201 the 2010-2014 seismic activity, with increasing and decreasing of slip values due to the temporal and spatial variation of the

202 recorded seismicity (Passarelli et al. 2015).

203

204

205 **~~2~~3 Seismotectonic Setting ~~framework~~**

206

207 **~~2.2 Earthquake/fault association and kinematics of the 2010-2014 seismic sequence~~**

208

209 ~~In the study area, the POL and the adjacent CAS faults (Fig. 1b) are the most studied structures from the seismotectonic point~~

210 ~~of view, as, based on the results of paleoseismological investigations (Michetti et al., 1997, 2000; Cinti et al., 1997, 2002),~~

211 ~~they are considered active and capable of producing strong earthquakes and surface faulting. In fact, a~~According to Michetti

212 et al.~~,~~ (1997, 2000) and~~;~~ Cinti et al.~~,~~ (1997, 2002), ~~the aforementioned literature, both the faults~~ POL and the adjacent CAS

213 faults were associated with at least two strong earthquakes, (M 6.5 and M 7.0), occurred in the period 2000-410 B.C. and 500-

214 900 A.D.~~.~~, respectively. The epicenter of the 8 January 1693 earthquake (M 5.3, CPTI15, Rovida et al., 2020, 2021; Fig. 1b,

215 Fig. 2) is also located within the hanging wall of the CAS and ~~in~~at the footwall of the MPR fault, some kilometers ~~km~~eastward

216 of the 2012 and 2014 Morano Calabro strongest events~~, then leading to exclude the MPR as the causative fault.~~

217 ~~The epicenter of the 8 January 1693 earthquake (M 5.3, CPTI15, Rovida et al., 2020, 2021; Fig. 1b) is also located~~

218 ~~within the hanging wall block of the CAS and in the footwall block of the MPR fault, some km eastward of the 2012~~

219 ~~and 2014 Morano Calabro strong events, then leading to exclude the MPR as the causative fault.~~

220 ~~Nevertheless, this event, which was first reported in the CFTI5Med Catalogue (Guidoboni et al., 2018, 2019) with M_w 5.7,~~

221 ~~was recently reduced to M_w 5.2 (Tertulliani and Cucci, 2014).~~

222 The epicenter locations of the M_w 5.5, 1708~~, (Rovida et al., 2021)~~ and M_w 5.1, 1894 earthquakes (Rovida et al., 2021), close

223 to the northern termination of the RSB and within its hanging wall, allows hypothesizing the latter fault as the possible

224 seismogenic source.

225 ~~For what concerns the instrumental seismicity, t~~The main instrumental event recorded in the Pollino area is the M_w 5.6 Mercure

226 earthquake (9 September 1998~~,~~; Fig. 1b), which was followed by some hundred aftershocks~~. Despite a preliminary attribution~~

227 ~~to the Castelluccio fault (Michetti et al., 2000), this earthquake~~ and that was associated by Brozzetti et al. (2009) with the SW-

228 dipping ~~CPST~~CSPT (Fig. 1b, Fig. 2), located some kilometers ~~km~~to the NE of the Mercure basin.

229 The focal mechanisms of the three strongest earthquakes (M_w 5.2, 25 October 2012-Mormanno; M_w 4.3, 28 May 2012-Morano

230 Calabro; M_w 4.0, 6 June 2014-Morano Calabro) are consistent with extensional (upper crustal) deformations (Montone and

231 Mariucci 2016; Mariucci and Montone 2020).

232

~~The 2010-2014 Pollino seismic sequence was triggered by extensional upper crustal deformations, as highlighted by the focal~~ ~~mechanisms of the three strongest earthquakes (M$_w$ 5.2, 25 October 2012 Mormanno, M$_w$ 4.3, 28 May 2012 Morano Calabro~~ ~~and M$_w$ 4.0, 6 June 2014 Morano Calabro).~~ All the associated WSW-ENE oriented T-axes are also quite ~~-~~parallel to the geological and seismological ~~minimum~~ least compressional axis, as provided by the tensorial analysis in the ~~neighboring~~neighbouring Mercure area (Brozzetti et al., 2009; Ferranti et al., 2017)~~,~~ or derived from borehole breakouts ~~investigations~~ (Montone and Mariucci, 2016; Mariucci and Montone 2020~~Montone et al., 2004; Pondrelli et al., 2006~~), and GPS data (D'Agostino et al., 2014). As discussed by Totaro et al. (2015, 2016) and Brozzetti et al. (2017a),

~~The~~ the available focal solutions ~~of the Pollino 2010-2014 seismic sequence, display W-dipping seismogenic planes which~~ well correlate with the Quaternary normal fault~~s~~ ~~segments~~ recognized in the epicentral area. ~~(see sect. 2.1). The coherence~~ ~~between field and seismological data is even more evident using the dataset provided by Totaro et al. (2015, 2016) and~~ ~~Brozzetti et al. (2017a) which suggest~~ represented by N-S to NNW-SSE-striking~~,~~ (W-dipping)~~,~~ seismogenic sources.

Correlating the hypocenters distribution ~~at depth~~ with the active faults ~~highlighted~~ at ~~the~~ surface, the seismogenic source of the 25 October 2012 Mormanno Earthquake (M$_w$ 5.2), ~~also responsible for the westernmost and larger seismicity cluster (Fig.~~ ~~1b),~~ is identifiable in both the segments of the WSW-dipping ROCS system (RSB and VCT in Fig. 1b, Fig. 2). These faults dip ~~at surface~~ 70°-75°, at the surface, and would reach~~,~~ ~~at depth,~~ a dip of ~55° at depth (Brozzetti et al., 2017a).

Through similar reasonings, the WSW-dipping MPR fault was suggested to be the causative fault of the eastern~~,~~ Morano Calabro~~,~~ cluster (Fig. 1b) and of its two major events (M$_w$ 4.3, 28 May 2012 and M$_w$ 4.0, 6 June 2014). ~~This~~ The fault extends for ~7 km in ~~the~~ a N170 direction and is co-axial with ~~the~~ the W-dipping nodal planes of the two main events of the sequence (Fig. 1b).

The partial reactivation of the CAS could be invoked to explain the minor ~~seismicity~~ cluster of seismicity recorded at the eastern side of the study area, although some of the events seem to ~~be located in~~be located in~~at~~ its footwall.

254

~~3~~ 4 ~~Material~~ Data and Methods

~~3~~4.1 Structural survey and fault kinematic analysis

257

We performed ~~A~~ a series of fieldwork campaigns, at 1:25.000 scale, in the study area and surrounding sectors~~neighbouring~~ ~~areas, between 2018 and 2020, were~~ ~~performed~~ to collect fault-slip data ~~in the study and neighbouring areas, at 1:25.000 scale.~~ ~~These measurements~~ ~~that~~ ~~were used~~ to ~~be~~ integrated with the geological-structural ~~data and to constrain the Quaternary~~ ~~extensional faults provided in~~observations reported ~~from~~in Brozzetti et al. (2017a). ~~In field, w~~We ~~initially used traditional~~ ~~structural analysis techniques. We integrated the data with data collected through digital mapping, by using~~ used the Fieldmove ~~app/software~~App (PetEx Ltd., version 2019.1) installed on a tablet computer to acquire the data in the field, and~~. All these data~~ ~~(shown in Fig. 2) were managed in a GIS database elaborated through~~ we managed them in ArcGIS v.10.8 (ArcMap©). Fig.

2 ~~also~~ shows the location of the ~~kinematic~~ survey sites ~~that are~~, considered structurally homogeneous outcrops ~~or groups of adjoining outcrops that fall~~falling within a maximum distance of 500 m~~, that is within the diameter of each small circle on the scheme (more detailed localizations in~~see also Supplementary Fig. 2).

The overall fault-slip dataset was first subdivided in minor and local homogenous kinematic subsets, the latter represented as pseudo-focal mechanisms using FaultKin 8 software (Marrett and Allmendinger, 1990; Allmendinger et al., 2012~~) (~~; Fig 3). ~~The obtained beachballs show the computed pseudo-focal mechanism each associated with a couple of average fault plane/average slip vector (Fig. 3) obtained through Bingham statistic analysis from the fault population collected in each survey site.~~

-The fault/slip data were subsequently inverted ~~in order to reconstruct the long-term (geological) stress field to be compared with the seismological tensor obtained from available focal mechanisms~~ (see following sec. 3~~4~~.~~2~~3)~~. Such comparison allowed verifying the persistence of the stress field over time, at least from the Middle Pleistocene to Holocene times~~.
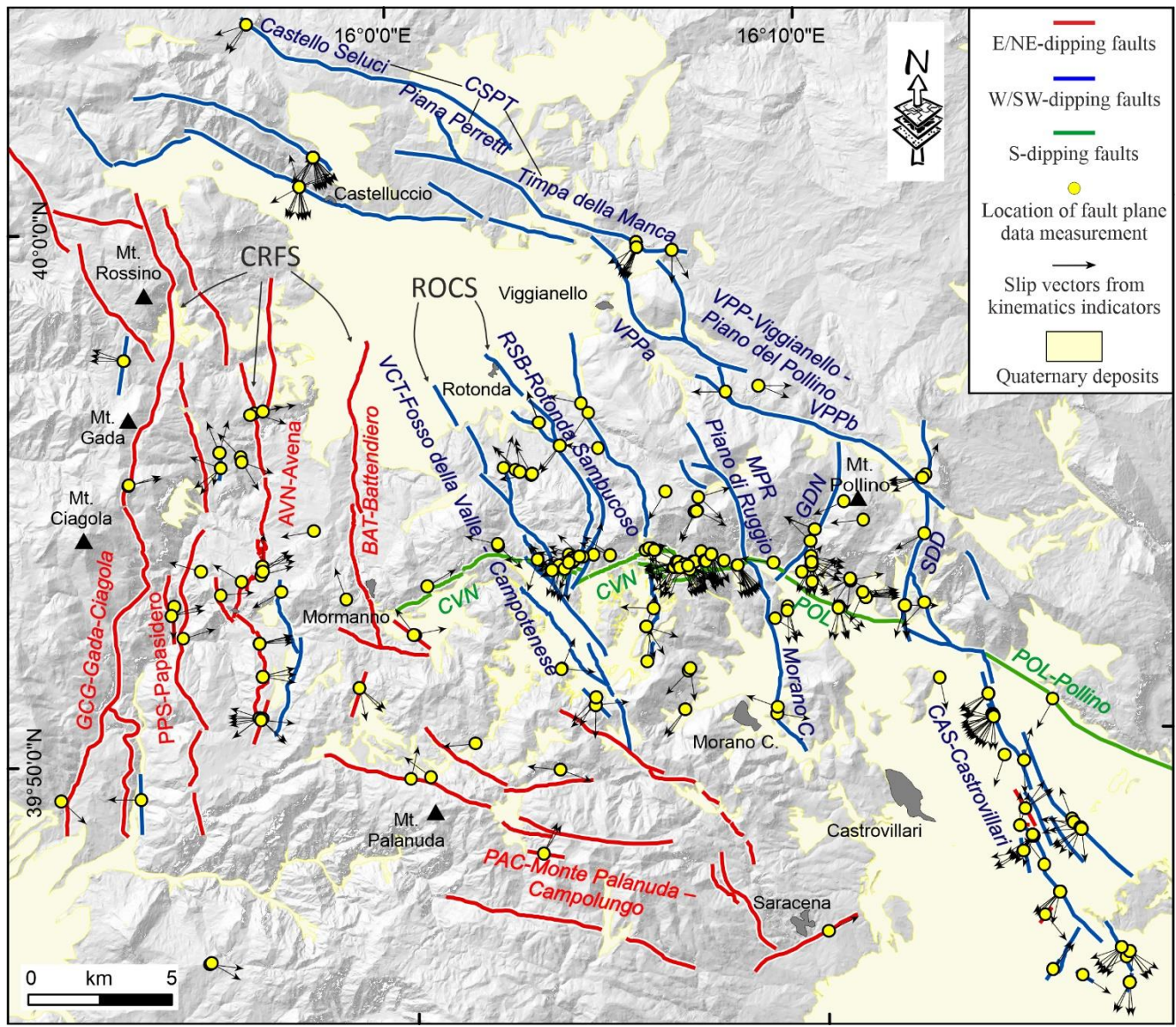
Figure 2: Structural Map at the Calabrian-Lucanian boundary (after Brozzetti et al., 2017a) with location of fault-slip data measurements. ~~Fault~~ Fault ~~k~~Key ~~for Fault names~~: CRFS= Coastal Range Fault Set; GCG= Gada-Ciagola fault; PPS= Papasidero fault; AVN= Avena fault; BAT= Battendiero fault; ROCS= Rotonda-Campotenese fault system; VCT= Fosso della Valle-Campotenese fault; RSB= Rotonda-Sambucoso; CVN= Cozzo Vardo-Cozzo Nisco fault; MPR= Morano Calabro-Piano di Ruggio fault; VPP= Viggianello - Pian~~oi d~~el Pollino fault set; VPPa= Viggianello-Prastio fault; VPPb= Vacquarro-Piani del Pollino fault; GDN= Gaudolino fault; POL= Pollino fault; CAS= Castrovillari fault; SDD= Serra Dolcedorme fault; PAC= Monte Palanuda – Campolungo fault; ~~CPST~~CSPT= Castello Seluci-Piana Perretti-Timpa della Manca fault.
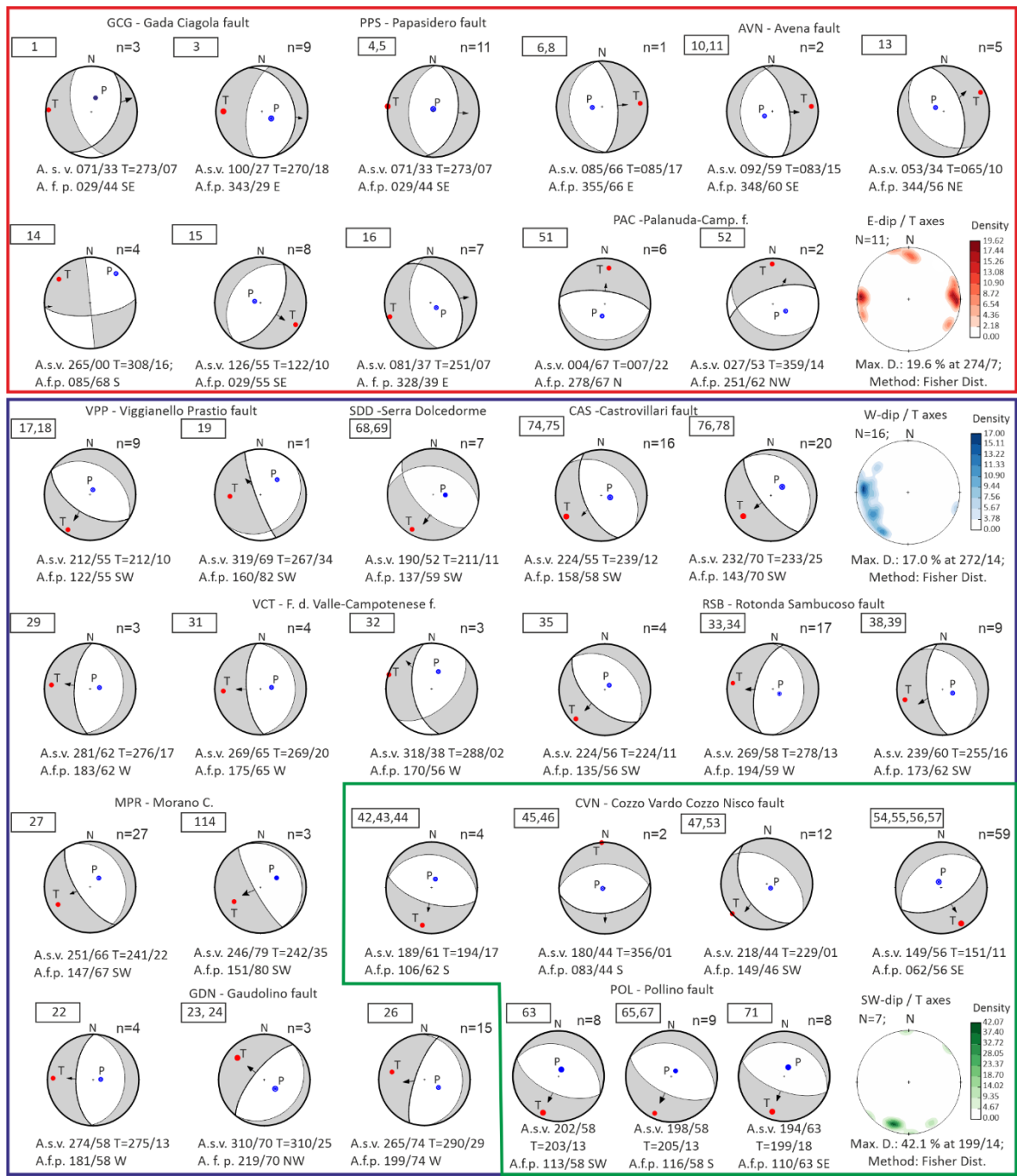
11

Figure 3: Kinematic analysis and pseudo-focal mechanisms obtained from fault/slip data using the FaultKin 8 software (Allmendinger et al., 2012). Pseudo-focal mechanisms are boxed with different colors on the basis of the fault system to which they belong to (color key as in the map of Fig. 1, Fig. 2). For each fault system, the density contour of the T-axis computed for each focal mechanism is reported (lower hemisphere projection). A.s.v.=Average striae value, A.f.p.=Average fault plane,

296　n=number of fault-plane measurements. Numbers in the rectangles (top left of each focal mechanism) refer to the group of
297　fault/slip data belonging to or neighbouring of a single site (location in Supplementary Fig. 2).

298

299　**3.2 Geological and seismological stress tensor inversion**

300

301　To investigate the coherence between the geological and the present-day (seismological) stress fields, we applied stress tensor
302　inversions to the available fault-slip data (Fig. 2, 3) and focal mechanisms (Fig. 4).
303　We used the inversion procedure proposed in Delvaux and Sperner (2003; Win-Tensor software) and applied it, separately, on
304　the different datasets. The procedure attempts to compute the orientation of the three principal axes of the stress ellipsoid ($\sigma 1$,
305　$\sigma 2$, $\sigma 3$) and the stress ratio $\Phi = (\sigma 2-\sigma 3)/(\sigma 1-\sigma 3)$ that optimize the misfit Function (*i.e.*, F5). The latter is built to i) minimize
306　the slip deviation between the observed slip line and resolved shear stress (30° misfit value is not expected to be exceeded),
307　and ii) favor higher shear stress magnitudes and lower normal stress to promote slip on the plane.
308　The inversion procedure provides for the preliminary (kinematic) analysis of data using an improved version of the Right
309　Dihedron method (Angelier and Mechler, 1977) to determine the starting model parameters (*e.g.*, the reduced stress tensor).
310　The stress ellipsoid is then computed through a 4D-grid-search inversion involving several runs during which the reduced
311　tensor is rotated around each stress axis, with a decreasing range of variability (from ±45° to ±5° and the full range of Φ values
312　is checked [0-1]). Each step attempts to find the parameters that minimize misfit function and that are used as a starting point
313　for the next run (see for details Delvaux and Sperner, 2003).
314　The geological data input consists of 268 quality-selected fault/slip data measured along the fault systems of the study area
315　(Fig. 2, 3). During the formal inversion, the same weight value was assigned to each fault giving the same quality factor
316　assigned to the slickenlines.
317　The seismological data input is represented (initially) by both nodal planes of each focal mechanism; afterward, the plane that
318　is best explained by the stress tensor in terms of the smallest misfit function is considered as the actual fault plane (Delvaux
319　and Barth, 2010).
320　The inverted seismological data are represented by focal mechanisms ($2.7 \leq M_w \leq 5.0$) taken from Totaro et al. (2015, 2016) and
321　reported in Fig. 4. An exponential weighting factor (corresponding to the earthquake magnitudes) has been assigned to account
322　for the prevailing kinematics of the most energetic events.
323　The final inversion (Fig. 5) includes only the fault- and focal-planes that are best fitted by a uniform stress field (Gephart and
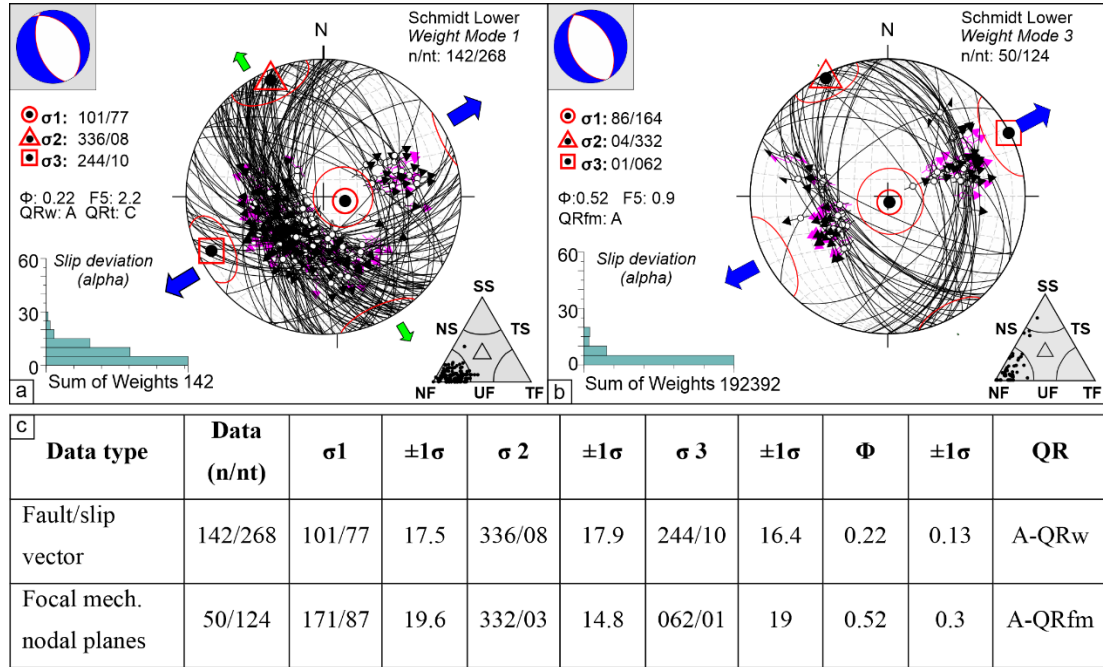324　Forsyth, 1984). The stress inversion results are shown in Fig. 5.

325
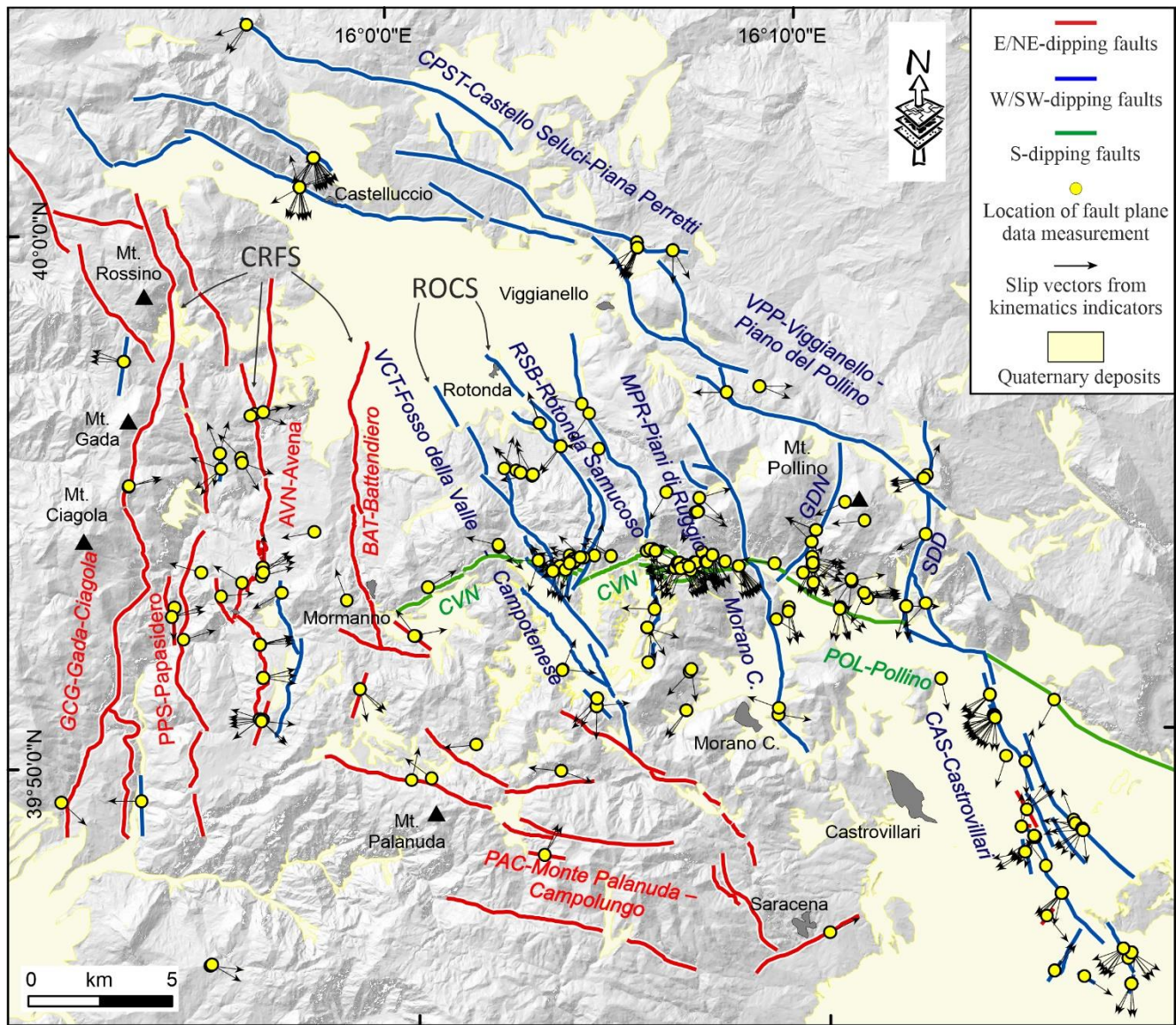
13

Figure 2: Structural Map at the Calabrian-Lucanian boundary (after Brozzetti et al., 2017a) with location of fault-slip data measurements. Fault Key: CRFS= Coastal Range Fault Set; GCG= Gada Ciagola fault; PPS= Papasidero fault; AVN= Avena fault; BAT= Battendiero fault; ROCS= Rotonda Campotenese fault system; VCT= Fosso della Valle Campotenese fault; RSB= Rotonda Sambucoso; CVN= Cozzo Vardo Cozzo Nisco fault; MPR= Morano Calabro Piano di Ruggio fault; VPP= Viggianello – Piano di Pollino fault; GDN= Gaudolino fault; POL= Pollino fault; CAS= Castrovillari fault; SDD= Serra Dolcedorme fault; PAC= Monte Palanuda – Campolungo fault; CPST= Castello Seluci Piana Perretti fault.
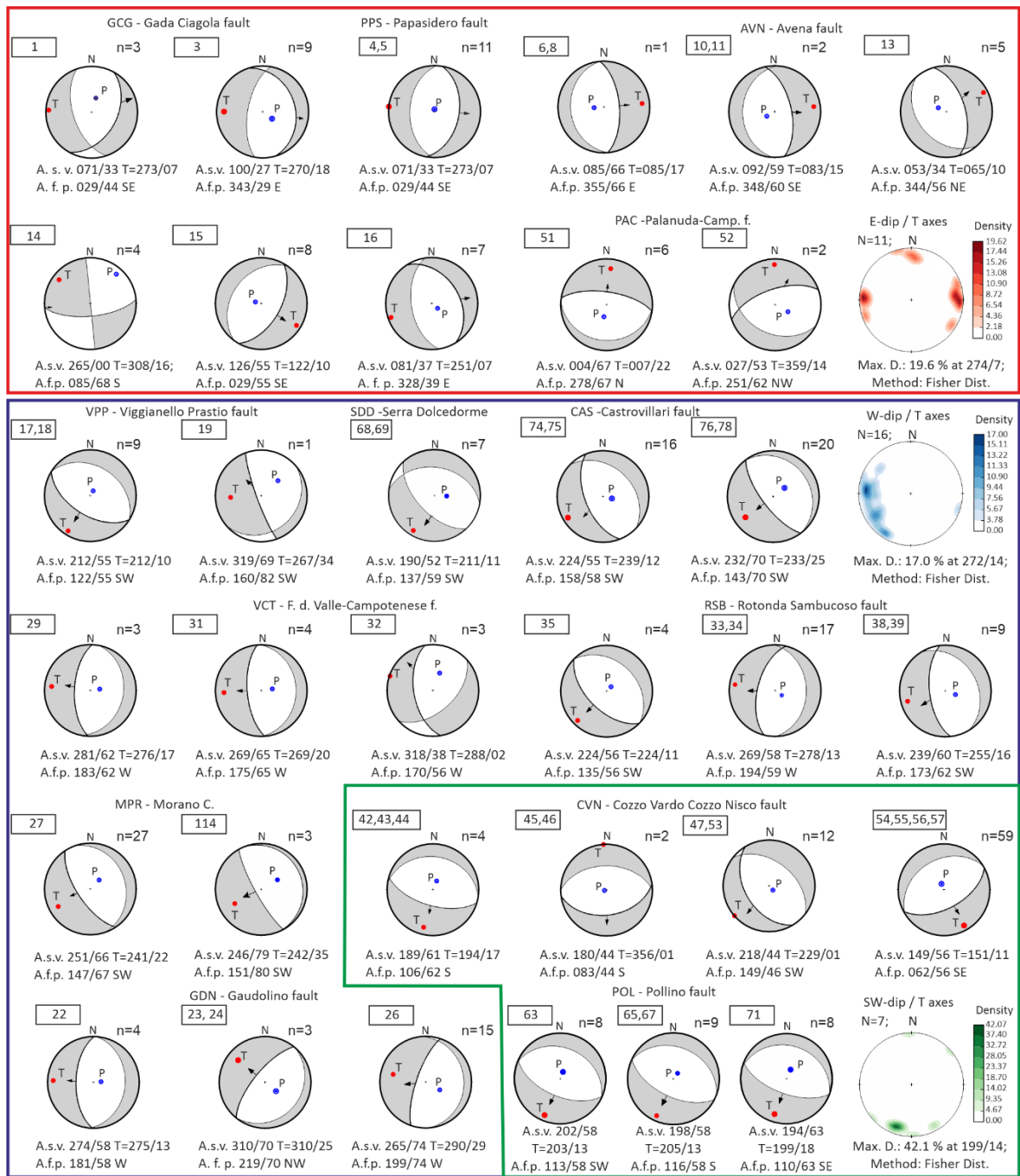
Figure 3: Kinematic analysis and pseudo-focal mechanisms obtained from fault/slip data using the software FaultKin 8 software (Allmendinger et al., 2012). Pseudo-focal mechanisms are boxed with different colors on the basis of the fault system to which they belong (color key as in the map of Fig.ure 1, 2). For each fault system the density contour of the T-axis computed for each focal mechanism is reported (lower hemisphere projection). A.s.v.=Average striae value, A.f.p.=Average fault plane.

341 ~~Numbers in the rectangles (top left of each focal mechanism) refer to the group of fault/slip data belonging to or neighbouring~~
342 ~~of a single site (location in Figure Supplementary 2).~~

343

344

16

c	Data type	Data (n/nt)	σ1	±1σ	σ 2	±1σ	σ 3	±1σ	Φ	±1σ	QR
	Fault/slip vector	142/268	101/77	17.5	336/08	17.9	244/10	16.4	0.22	0.13	A-QRw
	Focal mech. nodal planes	50/124	171/87	19.6	332/03	14.8	062/01	19	0.52	0.3	A-QRfm

34.3 2 Hypocenter location

To better characterize the 3D features of the tectonic structures located lying in the study areregion of the Mercure Pollino sequence and to frame it in the geological scenario of the Calabrian-Lucanian border, we performed a high-quality hypocenter locations. In previous works by Totaro et al. (2013 and 2015) and Brozzetti et al. (2017a), focused on the Mercure Pollino sequence, the seismicity occurred in the time period 2010-2014 was analyzed. This allowed the authors to well characterize the seismic activity and to provide preliminary interpretations for geological features of the study area.

In this study, wWe sensibly enlargedd, with respect to previous works by Totaro et al. (2013, 2015) and Brozzetti et al. (2017a), the time window for earthquake analyses, (i.e., with the data for all the earthquakes that occurred in the area between January 2010 and October 2018) selecting earthquakes with (local magnitude greater than 1.0 and hypocentral depth range 0-30 km) collected from the Istituto Nazionale di Geofisica e VulcanologiaINGV (www.ingv.it/INGV) Bulletin and the University of Calabria database (www.ingv.it, last access: 19 april 2021; http://www.sismocal.org, last access: 19 april 2021 /….)). Automatic and manually revised P- and S-wave arrival time picks have been selected for this dataset. The recording network, including both temporary and permanent stations managed by the University of Calabria and INGV (D'Alessandro et al., 2013; Margheriti et al., 2013), consisted of 61 stations with a maximum epicentral distance of 150 km (Supplementary Fig. 1). We computed accurate absolute hypocenter locations by applying first the non-linear Bayloc earthquake location algorithm (Presti et al., 2004, 2008) and subsequently the double-difference relative location method HypoDD (v.2; Waldhauser, 2001), and using the 3D P-wave velocity model by Orecchio et al. (2011). The Bayloc algorithm gives for each earthquake a probability density cloud with shape and size related to the main factors involved in the location process (e.g., network geometry, picking errors), and allows a generally more accurate estimate of hypocenter parameters and location uncertainties with respect to the more commonly used linearized location methods (see e.g., Lomax et al., 2000; Husen and Smith, 2004; Presti et al., 2008). The application of the Bayloc algorithm to the collected dataset provided, on average, horizontal and vertical errors of the order of 1.0 and 1.5 km, respectively, and allowed allowing us to obtain a well-constrained database that has been used as starting point for the subsequent analyses. As the second step, we applied apply the HypoDD algorithm, which minimizes phase delay-time residuals between pairs of events recorded at common stations (Waldhauser and Ellsworth, 2000). We computed the delay times from each event to its 30 nearest neighbors within 10 km distance, and to further ensure the robustness of the double-difference inversion. O only event pairs with at least eight phases observed at common stations were used. The final relocated dataset consists of 3109 events (Fig. 4 and Supplementary Fig. 1).

During the decade bBefore the 2010-2014 Pollino sequence, the instrumental data available within a range of nearly 75 km from the Mercure basin, referred to background seismic activity (Frepoli et al., 2005; Castello et al., 2006; Brozzetti et al., 2009). In this framework, the onlyA phases of significant seismic activity which affected the region, were the above mentioned 2010-2014 Pollino sequence (Fig. 4 and Supplementary Fig. 1) and was the moderate magnitude 1998-1999 Mercure seismic sequence that developed in the northern part of the homonym Quaternary basin (Supplementary Fig. 1; Guerra et al., 2005; Arrigo et al., 2005; Brozzetti et al., 2009) and). It started on September 1998 and lasted several months, showing showed some

similarities to the recent Mercure-Pollino sequence (*e.g.*, prevalent kinematics of focal mechanisms and hypocentral depth range). We explored the data available for this seismic activitysequence, in order to compute a high-quality earthquake location, following the procedure already described above for the 2010-2018 seismic activityearthquakes dataset. Since the recording network operating during the 1998-1999 seismic phase was significantly different from today, in terms of number of stations deployed in the region and their spatial distribution, the available data do not allow to reach the high level of constrain needed to perform the 3D structural model reconstruction.

410
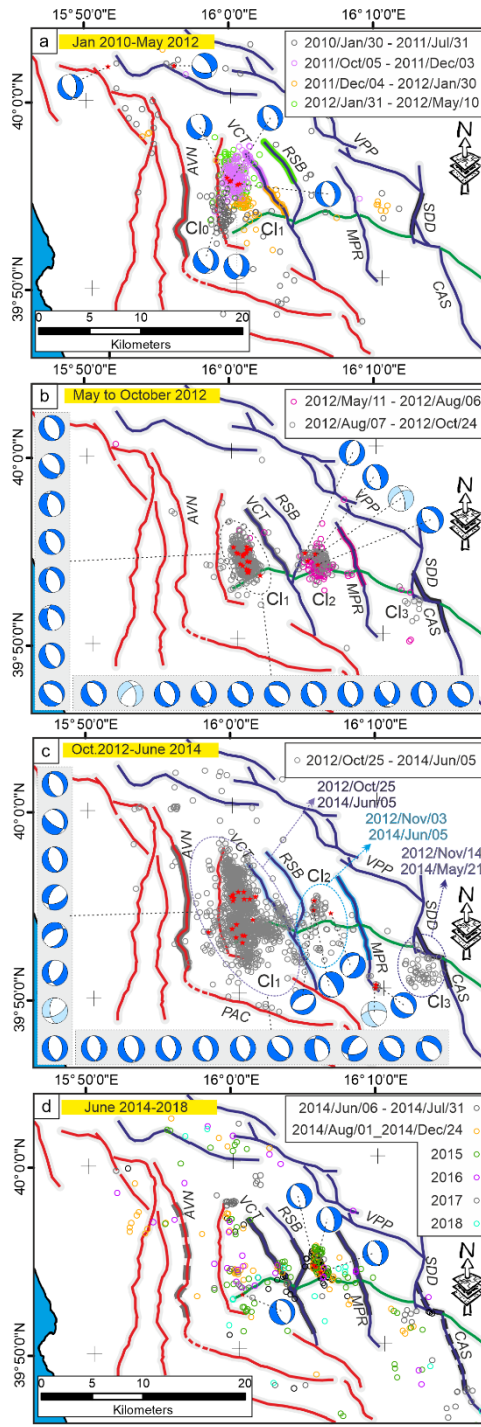
Figure 4: Time-space evolution of the 2010-2018 seismic activity in the Pollino area. Each panel shows the distribution of focal mechanisms (Totaro et al., 2015, 2016) and epicenters concentrated in a series of neighbouring clusters numbered as Cl ~~uster~~ 0, 1, 2, and 3 ~~(Cl0, Cl1, Cl2, Cl3)~~ from west to east, according to their activation time. See ~~the main text (~~section 4~~5~~.2~~)~~

20

for the sequence description. The Focal mechanisms are classified following Frohlich (2001) kinematics classification (blue beachball= Normal kinematics; light blue= Normal Strike kinematics). Red small circles represent the epicentres of focal mechanism solutions.

4.3 Geological and seismological stress tensor inversion

To investigate the coherence between the geological and the ~~present-day~~ (seismological) stress fields, we applied stress tensor inversions to the available fault-slip data (Figs. 2, 3) and focal mechanisms (Fig. 4).

We used the inversion procedure proposed in Delvaux and Sperner (2003~~; Win-Tensor software~~) and we applied it, separately, on the different datasets. The procedure ~~attempts to~~ computes the orientation of the three principal axes of the stress ellipsoid ($\sigma1$, $\sigma2$, $\sigma3$) and the stress ratio $\Phi = (\sigma2-\sigma3)/(\sigma1-\sigma3)$ that optimize the misfit Function (*i.e.*, F5). The latter is built to i) minimize the slip deviation between the observed slip line and resolved shear stress (30° misfit value is not expected to be exceeded), and ii) favor higher shear stress magnitudes and lower normal stress to promote slip on the plane.

The inversion procedure provides for the preliminary (kinematic) analysis of data using an improved version of the Right Dihedron method (Angelier and Mechler, 1977) to determine the starting model parameters (*e.g.*, the reduced stress tensor). The stress ellipsoid is then computed through a 4D grid-search inversion involving several runs during which the reduced tensor is rotated around each stress axis, with a decreasing range of variability (from ±45° to ±5°), and the full range of Φ values (0-1) is checked ~~[0-1]~~. Each step attempts to find the parameters that minimize the misfit function and that are used as a starting point for the next run (see for details Delvaux and Sperner, 2003).
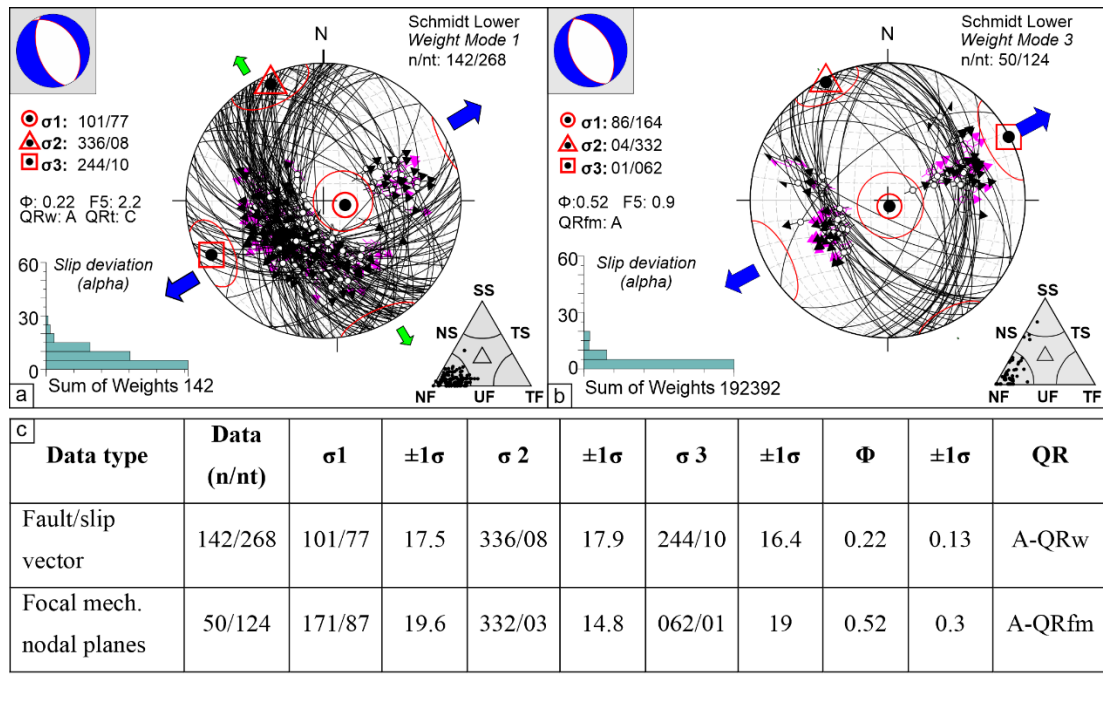
The geological data input consists of 268 quality selected fault/slip data measured ~~along the fault systems of~~ in -the study area (Fig. 2, 3). During the formal inversion, the same weight value was assigned to each fault ~~giving the same quality factor assigned to the slickenlines~~.

The seismological data input is represented (initially) by both nodal planes of each focal mechanism; afterward, the plane that is best explained by the stress tensor in terms of the smallest misfit function is considered as the actual fault plane (Delvaux and Barth, 2010).

The inverted seismological data are represented by focal mechanisms ~~(2.7≤M_w≤5.0) taken~~ from Totaro et al. (2015, 2016) and reported in Fig. 4. An exponential weighting factor (corresponding to the earthquake magnitudes) has been assigned to account for the prevailing kinematics of the most energetic events.

The final inversion (Fig. 5) includes only the fault- and focal-planes that are best fitted by a uniform stress field (Gephart and Forsyth, 1984).

Data type	Data (n/nt)	σ1	±1σ	σ 2	±1σ	σ 3	±1σ	Φ	±1σ	QR
Fault/slip vector	142/268	101/77	17.5	336/08	17.9	244/10	16.4	0.22	0.13	A-QRw
Focal mech. nodal planes	50/124	171/87	19.6	332/03	14.8	062/01	19	0.52	0.3	A-QRfm

Figure 5: Stress inversion results for the geological- (a) and seismological (b) data. On the lower hemisphere Schmidt nets, the pairs fault plane/slickenline pairs (a) and focal plane/kinematic indicators (rake) (b) are reported (great circles represent the fault planes; the dark and pink arrows indicate the measured slip directions (or rake) and resolved shears, stress respectively). The histograms represent the corresponding misfit angles vs. the number of data points; nt = total number of fault data; n = number of successfully inverted fault data; σ1, σ2, σ3 = principal stress axes; Φ = stress ratio = (σ2-σ3)/(σ1-σ3); the quality ranking factors (QR) and the stress inversion parameters with associated uncertainties (1σ standard deviations) are listed in panel (c). On the small upper left nets, the computed stress field represented as a focal mechanism is also reported. The triangles reported on the lower right corners of each panel (a) and (b) show the kinematic classification of data according to Frohlich (2001). (c) Geological and seismological stress tensor parameters computed starting from slip-vector measurements collected along the investigated fault systems (Figs. 2, 3) and 2.7<Mw<5.0 focal mechanisms, respectively (see. Sect. 3.3 and Fig. 4), respectively. Key: nt = total number of data (*e.g.*, plane/slickenline); n = inverted data; σ1, σ2, σ3 = principal stress axes; Φ = stress ratio = (σ2-σ3)/(σ1-σ3). QR = quality ranking: AQRw as in Sperner et al. (2003) and A-QRfm as in Heidbach et al. (2010).

34.4 3D Model building

The 3D Fault Model (3DFM) of the potentially seismogenic structures involved in the Pollino earthquakes was performed integrating the detailed Quaternary fault pattern provided in Brozzetti et al. (2009, 2017a) and integrated with new constrains from this paper, with the high quality 2010-2018 seismicity dataset.

We applied theFollowing the methodology defined by the Community Fault Model of Southern California (Nicholson et al.,

22

470 2014; Nicholson et al., 2015; Plesch et al., 2014)~~, which was also used, in previous works, to depict the subsurface geometry~~

471 ~~of the faults reactivated during~~also applied for recent Italian earthquakes (Lavecchia et al., 2017; Castaldo et al., 2018; Bello

472 et al., 2021a)~~.~~, we obtained the 3DFM of the Pollino area by integrating Quaternary fault mapping (Brozzetti et al., 2009,

473 2017a; this paper) with high-quality seismicity dataset (2010-2018), and by using~~,~~ the Move suite software v. 2019.1 (Petroleum

474 Experts Ltd).

475 ~~In the present work, the uncertainties in identifying the active fault segments and determining the fault earthquake~~

476 ~~associations were overcome thanks to the recent work of Brozzetti et al. (2017a) who discussed these aspects but without~~

477 ~~investigating the subsurface geometries of the sources.~~

478 ~~We obtained the latter by interpreting as seismogenic fault zone, the well-confined deformation volumes illuminated by the~~

479 ~~clustering of the hypocenters and using, for the 3D reconstruction, the Move suite software v. 2019.1 (Petroleum Experts Ltd).~~

480

481 ~~W~~In particular, we created several sets of closely spaced transects (~~half width~~distance=2 km) to cross and sample the

482 seismogenic fault zones in different directions (Fig. 6). The first two sets (oriented SW-NE and NW-SE) are respectively

483 ~perpendicular (*e.g.*, sections a, b in Fig. 6) and ~sub-parallel (*e.g.*, sections c-e in Fig. 6) to the ROCS (VCT and RSB), and

484 MPR active faults (*e.g.*, sections f in Fig. 6). A further NNE-SSW-striking set of transects was traced ~ perpendicular to the

485 active fault alignment bounding eastward the study area ~~affected by the 2010-2014 seismic sequence~~, which includes the

486 ~~CPST~~CSPT and VPP faults (sections g and h in Fig. 6).

487 The 3DFM building was carried out following three steps graphically depicted in Fig. 7 and synthetically described below.

488

489 *Step 1 - Extrusion of fault traces to shallow depth*

490 The traces of the Quaternary faults are ~~"extruded" along dip to reconstruct the so called "fault ribbons" (Fig. 7a) which~~

491 ~~are extrapolated~~ "extruded" to a pre-set depth of 2 km b.s.l, according to the ~~measured~~ fault planes dip measured in the

492 field~~ angle~~. In the absence of measured dip-angles, we assumed a fixed value of 60°. The obtained so-called "fault

493 ribbons" are rimmed upward by the topographic surface ~~represented as~~ (a 10 m-resolution DEM ~~(~~; Tarquini et al., 2012).

494 ~~In the model, they close at the fault tip and their relationships with the neighboring ribbons depend on the geometry of the~~

495 ~~transfer zone between adjoining faults.~~

496

497 *Step 2 - Down-dip extrapolation of the faults along seismological sections*~~:~~

498 Starting from the analysis of the seismological transects (Fig. 6), we traced the deep geometries ~~were traced~~ by connecting

499 the fault ribbons with the ~~the zones at depth where~~ seismicity clusters at depth ~~is denser~~ (Fig. 7b,c) downward to the base

500 of the seismogenic layer. ~~The latter, according to the model proposed in Brozzetti et al. (2017a), corresponds to an E-~~

501 ~~dipping basal detachment.~~

502 ~~We also considered the attitudes of the preferential fault planes from focal mechanisms falling within each section.~~

503

23

504

Step3 - Building of 3D fault surfaces through Delaunay triangulation method

This step allows reaching the final 3D reconstruction (Fig. 7c,d) by interpolating, through the Delaunay triangulation method (Delaunay, 1934Move software) all the elementsfault lines as interpreted along the seismological cross-sections (derived by the in the previous two sStep 2)s. The result is the fault plane surface that best approximates and connects the seismicity clusters of seismicity and the surface geology (represented by the fault traces extruded).

After joining at depth the fault ribbons with the subsurface sources, we obtained the seismogenic patches by projecting on each reconstructed fault plane the seismicity cluster as density contour (Fig. 7d).

This approach confirms that Cluster 1 and Cluster 2 well correlate respectively with the SW-dipping ROCS (RSB+VCT) and MPR faults. The westernmost concentration of hypocenters (*i.e.*, Cluster 0, Fig. 4a), given its location, may be due either to the deeper portion of the VCT fault or to the E-dipping AVN Fault, which act as the lower boundary of the W-dipping fault set (Fig. 7c,d).

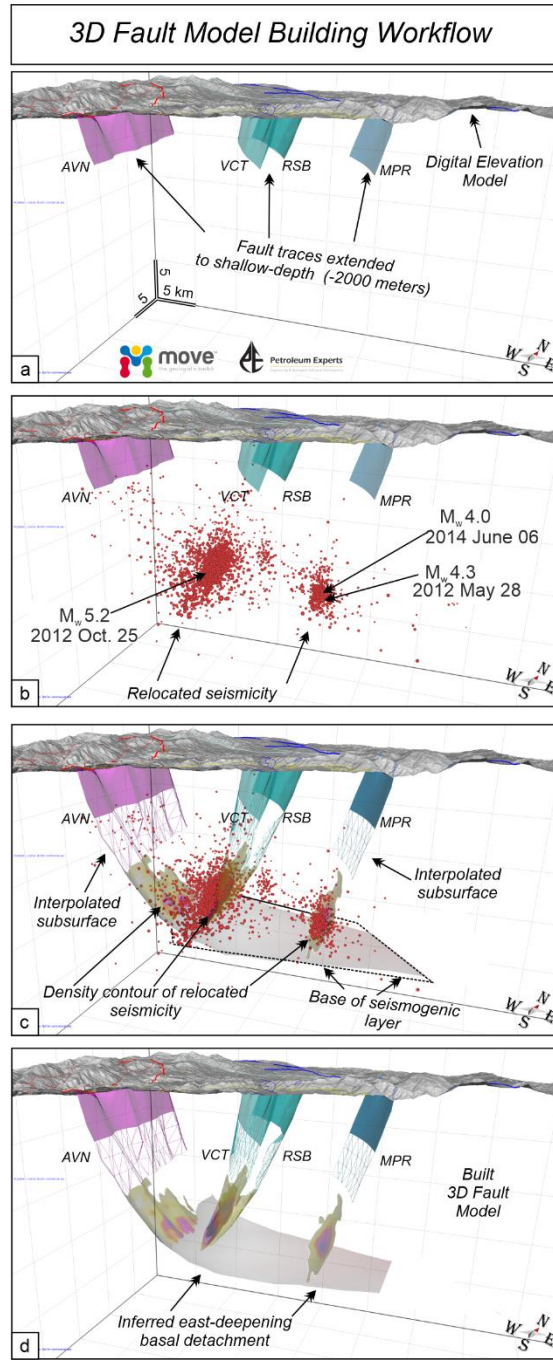We describe in detail the steps of the 3D model building of the seismogenic sources in the following sections.
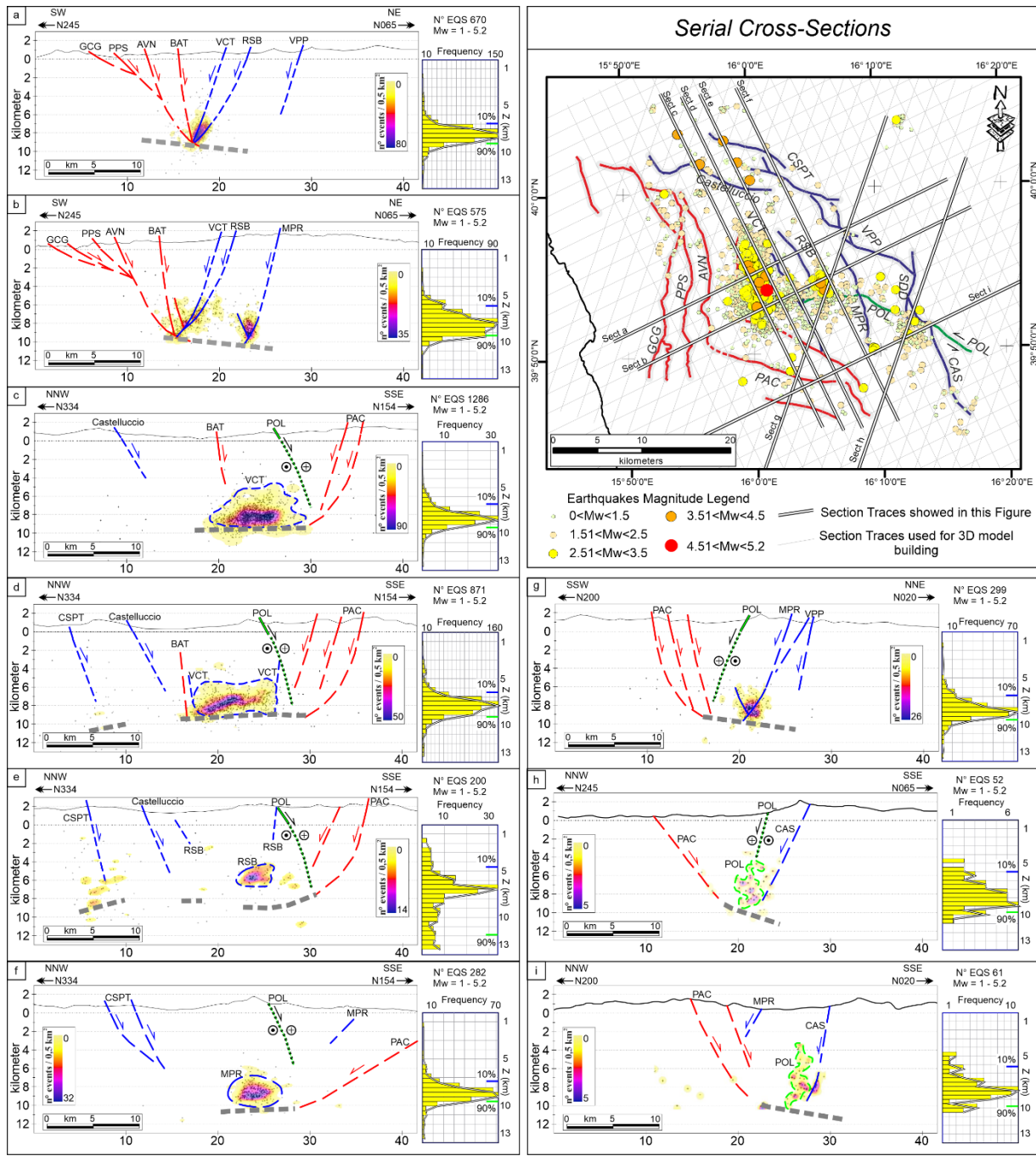
Figure 6: Epicentral map (map—upper--right panel) and hypocentral distributions (sections— a to -i) of the 2010-2018 seismic activity occurred in the Pollino area.— In the vertical cross-sections the earthquakes (grey dots) within a half-width of 1 km have been also reported also as density contours computed using Kernel Density Estimation. The histograms related to each close to each section shows the depth distribution of the hypocenters sequence. The traces of all the overall dataset of serial

cross-sections analyszed in this study are reported in map view (upper-right panel) as thin grey lines, while the bold lines relate
523   to the sections (a-j) shown in this figure.

524

Figure 7: 3D fault model building, from the surface (a 10 m-resolution DEM; from Tarquini et al., 2012) to the base of the
seismogenic layer. Faults acronyms as in Fig. 2. (a) "Fault ribbons" obtained by extruding the fault traces mapped at the surface

528 ~~up~~down to 2 km ~~b.s.l.~~depth, and~~,~~ considering the fault dip-angles measured in the field. (b) 3D fault model as in (a) with the
529 relocated seismicity. (c) Fault extrapolation at (seismogenic) depth through the clusters of hypocenters; ~~. t~~The modelled faults
530 connect the ribbons with the zones at the depth where concentrations of hypocenters ~~is~~are higher. The density contours of the
531 seismicity and the base of the seismogenic layer are also shown (see also panel d). (d) Final 3D fault model obtained integrating
532 the detailed Quaternary fault pattern with the high-quality 2010-2018 seismicity dataset.

533

534 **~~4~~5 Results**

535 **~~4~~5.1 Geological and Seismological Stress Tensors**

536

537 The computed geological stress tensor (Fig. 5) shows a relevant percentage of fault/slip vector pairs (~53%) consistent with a

538 uniform extensional stress field which is characterized by a N244 trending- and sub-horizontal σ3. The stress ratio

539 Φ=0.22±0.13 and the rank quality is QRw=A (ranking as in Sperner et al., 2003). Nearly all the kinematic axes related to the

540 inverted data belong to a normal-fault regime as also pointed out by ~~according to~~ the triangle in Fig. 5 ~~classification in~~ (Frohlich

541 (2001) ~~(see Fig. 5a)~~.

542 ~~It is worth noticing as 76% of the successfully inverted fault/slip vector pairs are related to the active fault planes belonging to~~

543 ~~the E- and W-dipping domains (Fig. 5a) while the remaining 24% include data related to the S-dipping system (CVN and~~

544 ~~POL). The latter evidence is consistent with the prevalent activation in the Late Quaternary of the E- and W-dipping fault~~

545 ~~systems.~~

546 The seismological stress tensor (Fig. 5b) obtained from inverting 50 actual fault planes (nt = 124 nodal planes), shows a normal

547 fault regime with an ENE-WSW trending and sub-horizontal σ3 (N062/01 ±19). The stress ratio Φ=0.52 ±0.3 and the rank

548 quality is QRfm=A (ranking as in Heidbach et al., 2010). Most of the nodal planes show normal-fault kinematics (see ~~the~~

549 ~~triangle diagram on the lower right corner of~~ Fig. 5b).

550 ~~Finally, i~~In both the inversions, a normal-fault regime with sub-horizontal and collinear (~SW-NE trending) σ3-axis has been

551 obtained. This result points out ~~confirms~~ the coherence between the geological (long-term) and the present-day stress field and

552 the persistence of this extensional regime at least since the Middle Pleistocene.

553 In addition, it is worth noticing as 76% of the successfully inverted fault/slip vector pairs are related to the active fault planes

554 belonging to the E- and W-dipping domains (Fig. 5a) while the remaining 24% include data related to the S-dipping system

555 (CVN and POL). The evidence together with the similarity between the computed stress tensors is consistent with the prevalent

556 activation, in the Late Quaternary, of the E- and W-dipping fault systems~~It is worth noticing as 76% of the successfully inverted~~

557 ~~fault/slip vector pairs are related to the active fault planes belonging to the E- and W-dipping domains (Fig. 5a) while the~~

558 ~~remaining 24% include data related to the S-dipping system (CVN and POL). The latter evidence is consistent with the~~

559 ~~prevalent activation in the Late Quaternary of the E- and W-dipping fault systems.~~

560

561

4.2 Time-space evolution of the Pollino sequence

The 2010-2018 seismic activity in the Pollino-Mercure area followed a peculiar evolution over time with epicenters concentrated in a series of neighboring clusters, numbered as Cluster 0, 1, 2, and 3, from west to east, according to their activation time. Such clusters, independent and unconnected to each other, are related to fault segments that are not in an along-strike continuity.

Cluster 0 (30/01/2010 - 31/07/2011), includes low magnitude ($1.0 \leq M_L \leq 2.9$) activity located in an NNE-SSW lengthened sector at the western boundary of the epicentral area. It is delimited westward by the more external segment of the E-dipping CRFS. In terms of generated events, this cluster was rather intermittent with periods characterized by moderate activity (Figs. 4a,c) alternating to substantially inactive ones (Figs. 4b,d). No significant seismicity occurred here during the 2015-2018 time span.

Cluster 1 started after 05/10/2011 and lasted for the entire 2010-2014 seismic activity. It extended continuously, either northward and southward, reaching a NW-SE length of ~12 km (Fig. 4a-c). It comprehends the higher number of earthquakes and is largely the major cluster as regards the wideness (~60 km^2) and energy release. It includes 30 events with $M_L \geq 3.0$ besides the 25 October 2012 strongest event of the whole Pollino seismic activity. During the 2015-2018 interval, Cluster 1 area was affected by low seismic activity, mostly distributed in its northern and southern portions; conversely, its central part, where epicenters were particularly dense between 2011 and 2014, became less active. Overall, the surface extent of Cluster 1, which partly overlaps with Cluster 0, is limited eastward by the W-dipping RSB and VCT faults. Its southern boundary nearly coincides with the southeastern continuation of the AVN fault (PAC, Fig. 4c).

Cluster 2 started in May 2012 in the sector between the two WSW-dipping RSB and the MPR faults. It elongates in N-S direction, for ~7 km to the northwest of the Morano Calabro town. Afterward, it was nearly continuously active, particularly during the periods May 2012 October 2014 (Fig. 4b,c); also in the period 2015-2018, significant seismicity persisted (Fig. 4d). Cluster 2 includes mainly low-magnitude events besides the strongest ones of 28 May 2012 and 6 June 2014 and three other earthquakes with $3.0 \leq M_L \leq 3.5$.

Further east, in the sector comprised between MPR and the alignment VPP-SDD-CAS faults, a minor cluster of seismicity (Cluster 3) develop since December 2011 (Fig. 4a). Since then (2011-2018) it was affected by poor and low-magnitude seismicity, which however was clearly above the threshold of background seismicity, with two $M_L=3.0$ events (Fig. 4a-d).

4.3 3D Fault Model building

Following the approach adopted and described in literature for the 3D fault model building (Lavecchia et al., 2017; Castaldo

et al., 2018; Bello et al., 2021a), we created several sets of closely spaced transects (half-width=2 km) to cross and sample the seismogenic fault zones in different directions (Fig. 6). The first two sets (oriented SW-NE and NW-SE) are respectively ~orthogonal (*e.g.*, sections 1, 2 in Fig. 6) and ~sub-parallel (*e.g.*, sections 3-6 in Fig. 6) to the ROCS (VCT and RSB), and MPR active fault. A further NNE-SSW-striking set of transects was traced ~orthogonal to the active fault alignment bounding eastward the area affected by the 2010-2014 seismic sequence, which includes the CPST and VPP faults (sections 7 and 8 in Fig. 6).

The 3DFM building was carried out following three steps graphically depicted in Fig. 6 and synthetically described below.

Step 1 Extrusion of fault traces to shallow depth

The traces of the Quaternary faults, belonging to both E- ad W-dipping sets (Fig. 7) are "extruded" (*i.e.*, projected downward three dimensionally) along dip to reconstruct the so-called "fault ribbons" (Fig. 7a). These latter are extrapolated to a pre-set depth of 2 km b.s.l, according to the dip angle of the fault planes measured at the surface during fieldwork campaigns both of this work and from previous literature (Brozzetti et al., 2009, 2017a). In the absence of these data, we assumed a fixed 60° dip angle. The obtained ribbons are rimmed upward by the topographic surface represented as a 10-m-resolution DEM (Tarquini et al., 2012). In the model, they close at the fault tip and their relationships with the neighboring ribbons depend on the geometry of the transfer zone between adjoining faults.

Step 2 Down-dip extrapolation of the faults along seismological sections:

Starting from the analysis of the seismological transects (Fig. 6), the fault extrapolation at depth is based on the assumption that the seismogenic volumes, (*i.e.*, the main clusters of hypocenters), illuminate the portion of the activated fault zones. In particular, the depth geometries were traced by connecting the surface "ribbons" (step 1) with the zones at depth where seismicity is more dense (*i.e.*, where the concentration of hypocenters is higher; Fig. 7b,c) downward to the base of the seismogenic layer. The latter, according to the model proposed in Brozzetti et al. (2017a), corresponds to an E-dipping basal detachment.

We also considered the attitudes of the preferential fault planes from focal mechanisms falling within each section. In general, this step is relatively simple in those cases where seismicity originates on fault zones having regular shape, whereas it gets complicated in areas, as the study one, where multiple faults, characterized by sharp strike changes, interact. In such cases, seismicity distributes in geometrically complex volumes and the hypocentre clusters have irregular contours, possibly because include groups of events generated on adjacent faults.

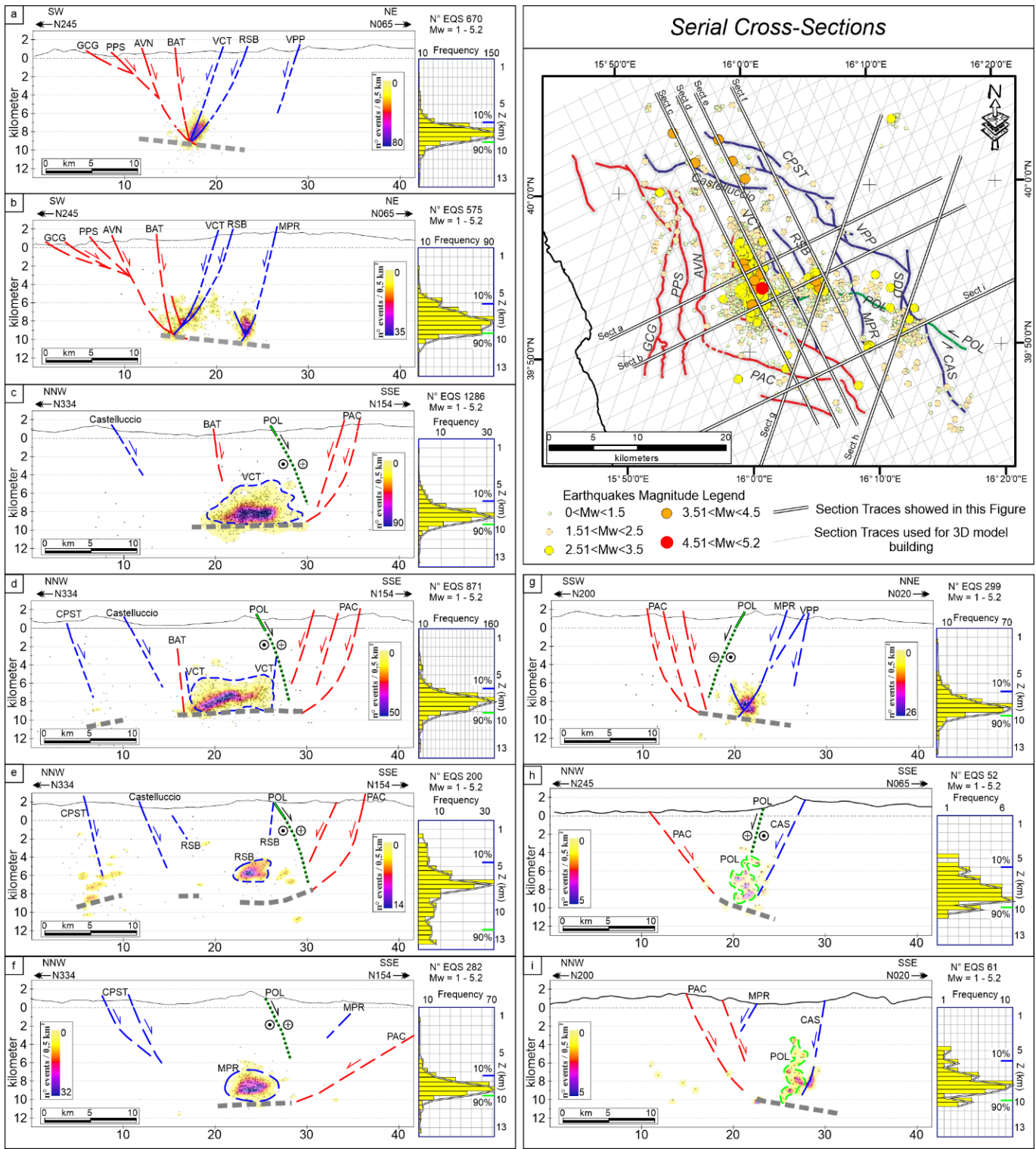*Step3 Building of 3D fault surfaces through Delaunay triangulation method*

This method automatically allows reaching the final 3D reconstruction of the seismogenic faults (Fig. 7c,d) by interpolating all the elements derived by the previous two steps.
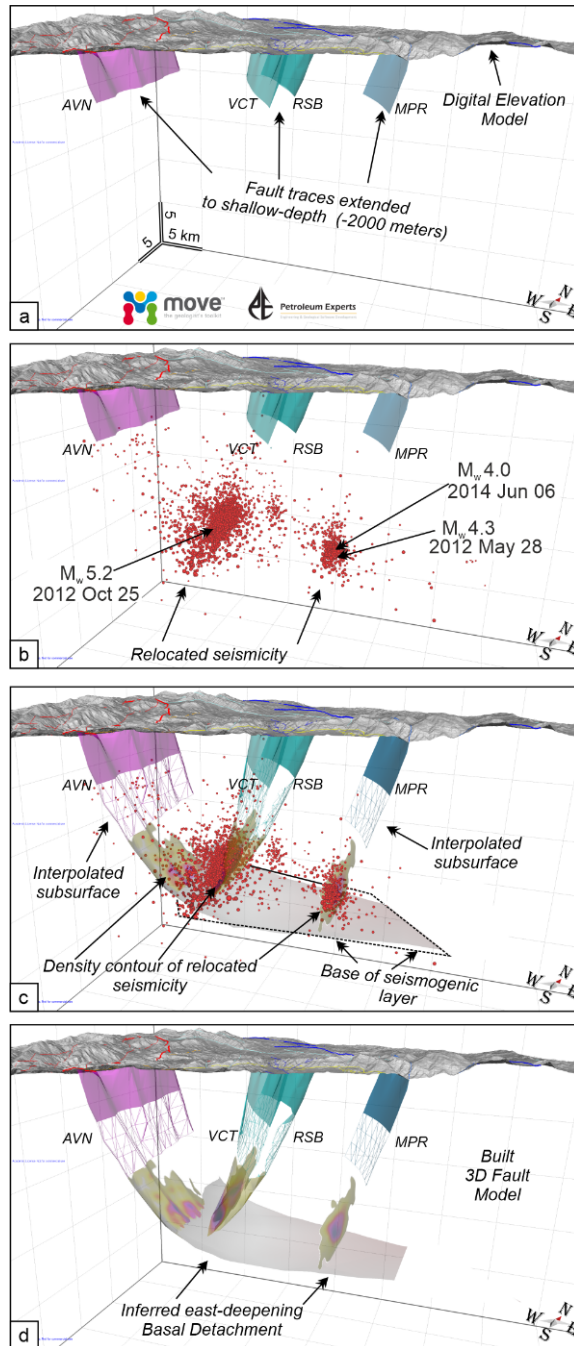
After joining at depth the fault ribbons with the subsurface sources, we obtained the seismogenic patches by projecting on each reconstructed fault plane the seismicity cluster as density contour (Fig. 6d). This depiction allows visualizing, with a good degree of approximation, the portion of the fault which released most of the seismicity during the considered time interval.

630   This methodology made it possible to refer with good confidence the hypocentral distribution of the 2010-2018 seismicity
631   to the causative faults confirming that Cluster 1 and Cluster 2 well correlate respectively with the SW-dipping ROCS
632   (RSB+VCT) and MPR faults. The westernmost concentration of hypocentres (*i.,e.*, Cluster 0), given its location, may be
633   due either to the deeper portion of the VCT fault or to the E-dipping AVN Fault, which act as the lower boundary of the
634   W-dipping fault set (Fig. 7c,d).
635

Figure 7: ~~3D fault model building, from surface (represented by a 10 m-resolution DEM – Tarquini et al., 2012) to the base~~
645 ~~of the seismogenic layer. Faults acronyms as in Figure 2. (a) "Fault ribbons" obtained by extruding the fault traces mapped at~~
646 ~~surface up to shallow depth (2 km b.s.l.), and considering the fault dip angles measured in the field. (b) 3D fault model as in~~
647 ~~(a) with relocated seismicity. (c) Fault extrapolation at (seismogenic) depth through the clusters of hypocenters. The modelled~~
648 ~~faults connect the ribbons with the zones at depth where concentrations of hypocenters is higher. The density contours of the~~
649 ~~seismicity and the base of the seismogenic layer are also shown (see also panel d). (d) Final 3D fault model obtained integrating~~
650 ~~the detailed Quaternary fault pattern with the high-quality 2010-2018 seismicity dataset.~~

651
652
653

654 **4~~5~~.~~4~~ 3 3D Fault Model of the Pollino area ~~Quaternary and active~~ fault system**

655

656   The 3DFM obtained ~~to the depth of ~10-12 km~~ (Fig. 8), ~~as well as including~~which includes the seismogenic fault system
657 ~~activated~~ involved during and after the 2010-201~~8~~4 Pollino seismic ~~sequence~~activity ~~(i.e., 2010-2018), represented by~~ (CRFS,
658 ROCS, and MPR) also~~, also~~ encompasses those faults (GCG, PPS, AVN, BAT, CSPT, VPP, SDD, CAS) that, while showing
659 no direct evidence of recent seismic activity, play a significant role in the seismotectonic frame of the area. ~~In other words,~~
660 ~~adjacent structures represent possible barriers to the propagation of coseismic faulting.~~
661 ~~We interpreted the~~ The westernmost fault structures (*i.e.*, GCG and PPS), whose deep geometry is not strictly constrained by
662 subsurface data, have been interpreted according to the structural extensional style proposed by Brozzetti et al. (2017a). Th~~is~~is
663 ~~is~~e latter is coherent with the reconstructions of the active extensional belt of the southern and central Apennines described in
664 the literature (Barchi et al., 2007; Amicucci et al., 2008; Brozzetti et al., 2011, 2017a, 2017b; Lavecchia et al., 2017).
665 Overall, this style is characterized by an asymmetric extension driven by a low-angle (20° to 35°) E-dipping detachment fault
666 which represents the basal decollement of all the other extensional structures.
667 In the model, all the faults are traced at the surface with their ~~outcrop~~ dip-angle as measured in outcrop and evolve downward
668 with nearly-listric geometries to join the detachment at increasing depth from west to east. The latter~~,~~ represents~~,~~ the
669 structurally controlled base of the seismogenic layer.
670 ~~We interpreted t~~The GCG (Figs 1b, 8), which crops out at low-angle and overcomes all the other east-dipping faults (in terms
671 of both slip and associate extension), ~~i~~as the currently inactive break-away zone of such a detachment.
672 The AVN and BAT (Figs 1~~b~~2, 8), which are the easternmost E-dipping splays, are suggested to be active and seismogenic,
673 being possibly the causative structures of the Cluster 0 of hypocenters ~~recognized during the 2010-2014 activity~~ (Fig. 4a).
674 ~~In such a model, the hypocenters of~~ Cluster 1 and Cluster 2~~,~~, which are downward confined by the E-dipping detachment,
675 confirm the activity of the W-SW-dipping ROCS and MPR faults, ~~which~~that we consider them the ~~main geological structures~~
676 involved during ~~sources of~~ the 2010-2014 seismic ~~sequence~~activity~~, furthermore are downward confined by the E-dipping~~
677 ~~detachment~~ (Figs. 4 and 8a,a1). ~~In such a model, also the W-SW-dipping ROCS and MPR faults, which we consider the main~~
678 ~~sources of the 2010-2014 seismic sequence, are downward confined by the E-dipping detachment (Fig. 8a,a1).~~
679 Further east, the 3DFM has been widened to include the W-dipping ~~CPST~~CSPT and VPP faults, considered the outer

680 seismogenic front of the extensional system ~~(Brozzetti et al., 2009~~, 2017a)~~.~~

681 ~~The yellow surface shown in Fig. 8c,d, depicts, in nearly frontal view, the 3D shape of the POL and its westernmost segment~~

682 ~~(CVN) bounding to the north of the Campotenese basin.~~ The along-strike continuity of ~~of~~ POL and CVN ~~this fault~~ is

683 interrupted by the W-dipping ROCS and MPR faults (Fig. 8c,d), coherently with the cross-cut relationships observed in the

684 field (Fig. ~~1b~~2).

685 ~~In Fig. 8d, t~~The de~~ep~~th geometry ~~of~~ of POL and CVN is ~~interrupts~~ interrupted by the NNE-dipping AVN (~~violet surface in~~

686 Fig. 8d) which acts as the southern and basal boundary of the entire active fault system.

687 Finally, ~~the comparison between~~ the ~~reconstructed~~ 3D ~~model~~FM ~~and the plotted re-located seismicity evidently~~ shows that

688 almost the whole 2010-2018 ~~hypocenters~~ seismicity correlate~~s~~ with the W-dipping structures but without affecting their

689 southern termination zones. In other words, no or very few events locate south of the intersection with POL and CVN faults.

690 This latter observation suggests that although the POL and CVN did not play an active role in ~~the origin of~~causing the

691 considered seismic ~~activ~~ity, they play a significant role in influencing its distribution.

692
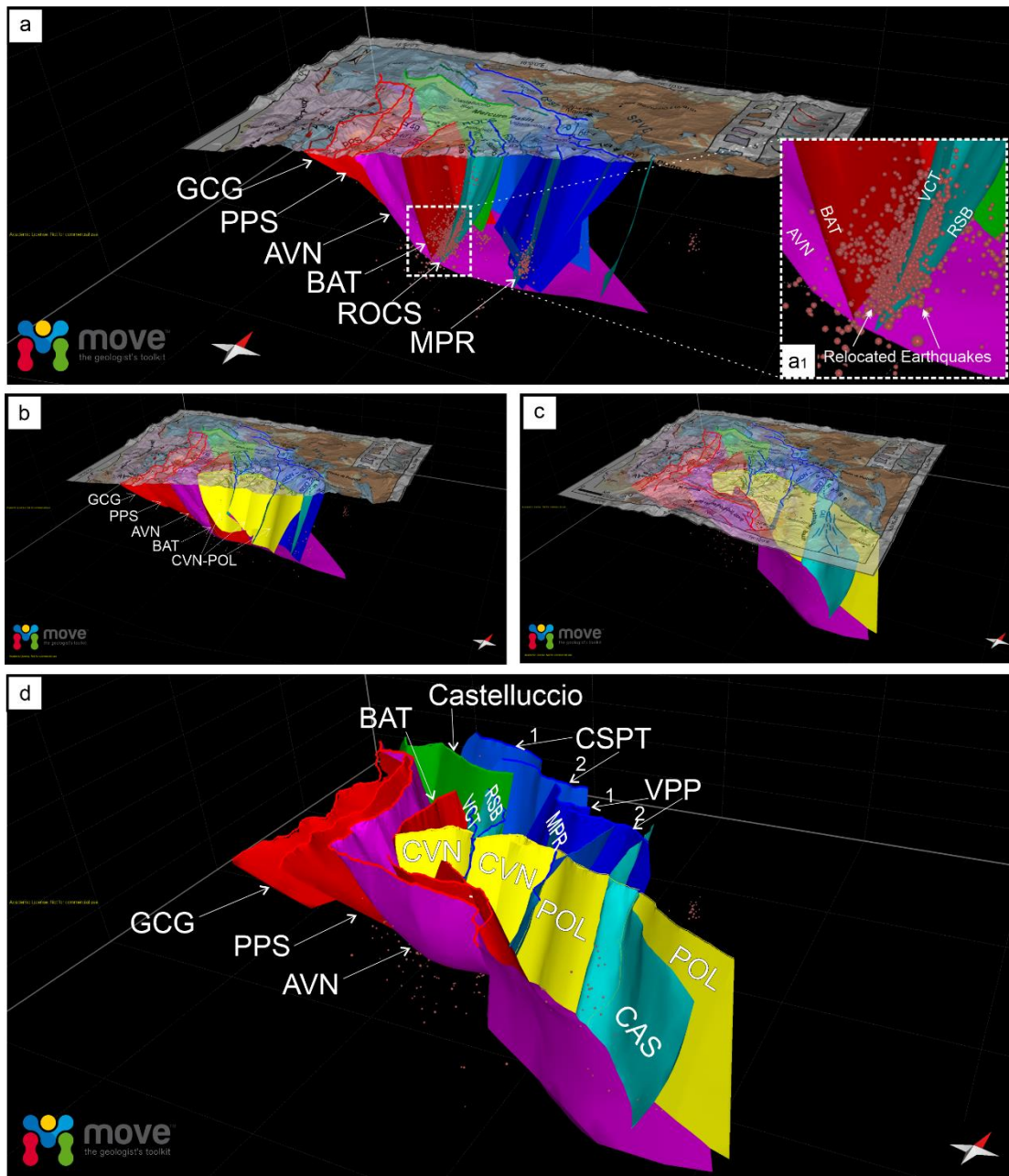
Figure 8: ~~TriThree dimensional model~~3D Fault Model of the extensional system at the Calabrian-Lucanian boundary extrapolated down to ~10-12 km. In the panels (a) (b) (c) the geological-structural map (from Brozzetti et al., 2017a) is superimposed over a 10 m-resolution DEM (from Tarquini et al., 2012). The reconstruction of the fault systems is discussed in the paper. In the top panel (a), the lower right inset (a1) shown the ~~of the top panel (a),~~ detail of the main faults involved ~~in~~during the 2010-2018 seismic activity ~~is shown~~. (d) 3DFM of all extensional fault realized through the move software, for the acronyms see supplementary text 1.~~3DFM of the extensional system at the Calabrian Lucanian boundary extrapolated~~

701 ~~down to the depth of ~10-12 km. The g~~Geological-structural map used as a base over a 10 m-resolution DEM is ~~(from Brozzetti~~
702 ~~et al., 2017a). superimposed over a 10 m-resolution DEM (from Tarquini et al., 2012) with the downdip reconstruction of the~~
703 ~~fault systems discussed in the paper. In the lower right inset (a1) a detail of the main faults involved in the 2010-2018 seismic~~
704 ~~activity is shown.~~
705 ~~Fault surfaces are those belonging to the seismogenic fault system activated during and after the Pollino seismic sequence~~
706 ~~(2010-2018), and those playing a key role in the seismotectonic context of the area.~~ The faults belonging to the E-NE-dipping
707 CRFS fault set are represented in red and violet, whereas the antithetic ROCS and MPR faults are shown as blue surfaces (fault
708 acronyms as in ~~Figure~~ Fig. 2). ~~Yellow~~ The yellow surface is the ~~tri~~three-dimensional surface of the POL and its westernmost
709 segment (CVN) bounding, to the north, the Campotenese basin.
710
711 ~~5 6~~ Discussion
712
713
714 ~~565.1 4~~ From 3D Fault Model to expected earthquake magnitude
715 ~~Maximum expected magnitude~~
716
717 Coherently with what is observed in most of the Apennine chain (Montone and Mariucci, 2016; Mariucci and Montone, 2020),
718 the upper crustal Pollino seismicity develop~~sed~~ in response to WSW- ENE oriented extension. This is well constrained by the
719 focal solutions of the strongest events (M_w 5.2, 25 October 2012; M_w 4.3, 28 May 2012, and M_w 4.0, 6 June 2014 earthquakes)
720 and of all the $M_w \geq 3.5$ earthquakes that occurred during the 2010-2014 ~~seismic sequence.~~
721 ~~The tensor provided by the~~, and with the results of the geological and seismological inversion ~~of fault/slip data, (collected~~
722 ~~on the Quaternary faults (Figs. 2, 3 and~~ Fig. 5a)~~., is also extensional and nearly co-axial to the seismological one.~~ Such
723 consistency suggests that the present stress field is in continuity with the long-term one, which ~~is active~~set up at least since
724 the Early-Middle Pleistocene, ~~as already suggested by previous works (Papanikolaou and Roberts, 2007; Brozzetti et al. 2009;
725 2017a).
726 Comparing the distribution of the whole 2010-2018 seismic activity with the Late Quaternary structures mapped at the surface,
727 we maintain that the ROCS and the MPR faults are ~~respectively~~ suitable as the seismogenic sources for the Mormanno (2012,
728 M_w 5.2) and Morano Calabro (2012, M_w 4.3 and 2014, M_w 4.0) earthquakes, respectively.
729 ~~However~~In addition, ~~the~~ our 3DFM ~~goes beyond establishing the earthquake-structure associations and~~ allows ~~defining~~ a
730 ~~strictly constrained~~ parameterization of the sources and ~~assessing~~ their seismogenic potential assessment.
731 ~~From the overall fault model of Fig. 9a (the same of Fig. 8 but in zenithal view) we extracted the plan view of the W-dipping~~
732 ~~seismogenic faults (Fig. 9b). This~~ The ~~in plan~~map view of the W-dipping faults ~~of our 3D model~~ (Figs. 9a,b) ~~representation~~
733 depicts irregularly-shaped seismogenic boxes which are ~~bordered~~ delimited to the east by the fault traces (at the surface) and~~,~~
734 ~~on the opposite side, to the west~~ by ~~the projection at the surface of the~~ branch line of each fault ~~from~~ with the base of the
735 seismogenic layer. Some of ~~the aforementioned~~ these boxes include historical or instrumental earthquakes (~~colored squares in~~
736 Fig. 9b) while others are not associated with any significant event.

36

The performed 3D reconstruction allowed us ~~to precisely estimating~~ estimate the effective area extent of all the fault segments~~,~~ ~~despite their irregular shape and complex segmentation pattern. The calculated areas~~ (Fig. 9c ~~left white column~~), that, when inserted in the appropriate scaling relationships, provide the ~~maximum~~ expected magnitude possibly releasable~~that each fault might release~~ in ~~the borderline~~ case ~~in which the coseismic~~of entire rupture ~~affects its entire plane~~ (Fig. 9c~~, yellow, blue, and brown columns~~).

We also computed T~~the maximum~~ magnitude values obtained using the regressions as a function of the surface fault length (Fig. 9c)~~., right white column) are listed in Fig. 9c (light blue, green, and grey columns)~~.

Using six different empirical relations (Wells and Coppersmith, 1994; Wesnousky, 2008; Leonard, 2010; Stirling et al., 2013)~~Finally, the two graphs of Figs. 9d (fault area based scaling relationships) and 9e (fault length based scaling relationships) allow~~ we compar~~ing~~ the values determined, for all the investigated active normal faults (Figs. 9d,e)~~., using six different empirical relations (Wells and Coppersmith, 1994; Wesnousky, 2008; Leonard, 2010; Stirling et al., 2013)~~.

It is evident that, for each fault, the ~~maximum~~ expected magnitude ~~reported in Fig. 9d (~~computed using fault area~~)~~ is lower than ~~that~~ the one ~~plotted in Fig. 9e (~~computed by using fault length~~.)~~ ~~and also t~~The range of variation ~~(length of yellow bars on Figs 9d and 9e graphs)~~ is narrower for the values computed on the ground of fault-area regressions (yellow bars in Figs. 9d,e).

Given the significant difference in the magnitude values computed using area- or length-based scaling relationships, we suggest that (where possible) the reconstruction of a 3D-fault geometry should be pursued and preferred in order to derive more reliable parameters to be used~~As the difference between area- and length based relations in the obtained results is significant, a matter of primary importance concerns which scale relationships are to be used for the evaluation of the maximum expected magnitudes.~~
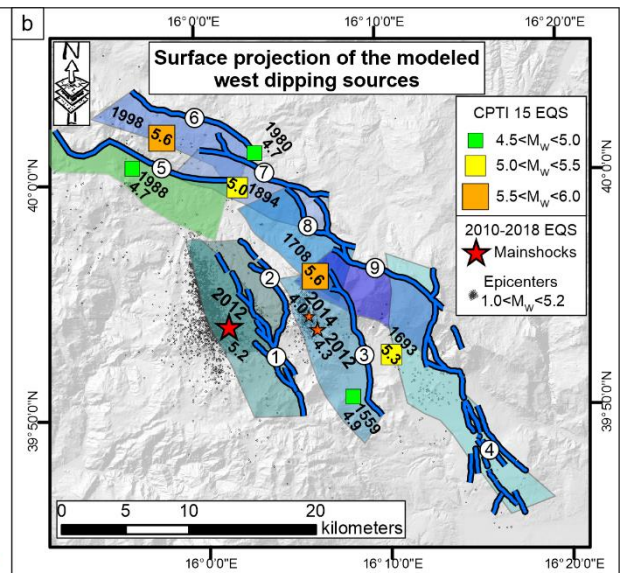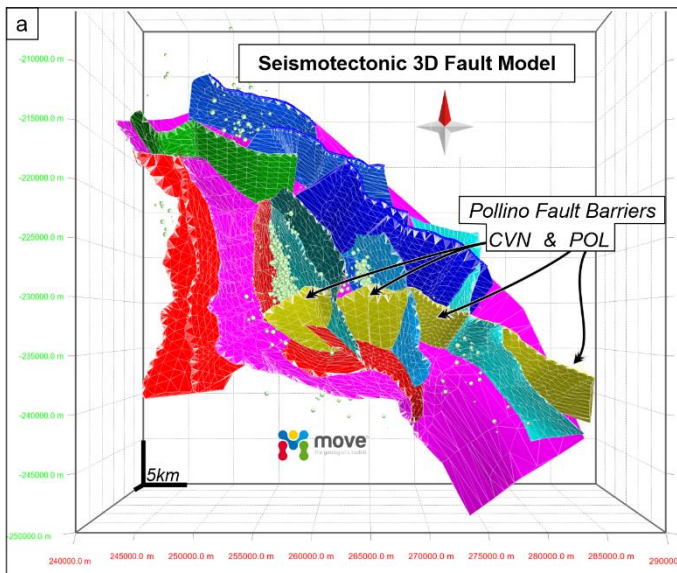
~~I,~~in the light of our results, we suggest that, wherever possible, the selection must be made taking into account~~considering the 3D reconstructed geometry of the faults, which allows determining as precisely as possible its shape~~s ~~and parameters~~ (Supplementary Table 1).

This is even more essential in complex extensional systems as~~following~~~~particularly correct for the observation that, as shown, T~~the ~~extensional faults system of~~ the one we investigated along the Calabrian-Lucanian border~~that, as shown, is markedly asymmetrical, namely characterized by high-angle W-dipping active faults, delimited downward by an E-dipping, low angle, detachment fault from which the high angle active splays branch upward (Brozzetti, 2011; Brozzetti et al., 2017a, 2017b). It is characterized by high angle W-dipping active faults (ROCS, MPR, VPP, CPST and CAS, Fig. 8a-d) delimited downward by an E-dipping, low angle, detachment fault (violet surface in Fig. 8a) from which the high angle active splays (AVN and BAT, Figs. 7,8) branch upward.~~

In fact, T~~the 3D~~ ~~reconstruction of the fault system model~~FM highlights ~~that~~as the areal extension of the ~~depth reached by the~~ W-dipping faults, ~~which strictly influence their areal extension,~~ depends on their position within the hanging wall of the detachment (see sect. 5.3). ~~In other words,~~This implies that faults with comparable length at the surface may have significantly different areas, depending on the reached depths.

771 The ~~CPST~~CSPT, VPP and CAS ~~belong to the easternmost extensional alignment and~~ crop out at great~~est~~ distance from the

772 GCG break-away zone. Consequently, they intersect ~~at the higher depth of~~ the basal detachment at the higher depth and have

773 the maximum area extent among the W-dipping fault set (Fig. 9a,d)~~. implying, in turn, different values of the maximum~~

774 ~~expected magnitude.~~

775 ~~From the previous reasoning, it follows that the 3DFM, which allows estimating accurately the subsurface extent and areas of~~

776 ~~the seismogenic faults, leads to prefer for the assessment of the associate seismogenic potential, the scaling relationships based~~

777 ~~on the fault area.~~

778 ~~In our case~~I, ~~b~~By applying ~~this type of regressions~~ the afore mentioned scaling laws (Fig. 9) to the W-dipping faults identified

779 to be ~~the sources~~involved during ~~of~~ the 2010-2014 seismic ~~sequence~~activity, we calculated the ~~maximum~~ expected magnitude

780 of ~M_w=6.1 for the VCT and the RSB, and of ~M_w= 6.2 for the MPR. Since the two faults (RSB+VCT) of the W-dipping

781 ROCS has been interpreted to join at hypocentral depth to form a single structure (thus a unique seismogenic patch was

782 reconstructed – Fig. 10a), ~~A~~a value of ~ M_w=6.4 could be reached in the case of ~~the~~a complete and concurrent ruptures on

783 both the ~~ROCS~~ segments ~~(joined RSB+VCT)~~.

784 ~~It is noticeable that t~~The aforesaid values are sensibly higher than the magnitudes of the earthquakes recorded to date in the

785 Mercure-Campotenese area (Figs. 1b, 9b), thus suggesting that the considered faults may have released only partially their

786 seismogenic potential during historical times.

787 This inference also agrees with the distribution and evolution of the 2010-2018 seismic activity. The clusters of the relocated

788 hypocenters concentrated in the deepest parts of the ROCS and MPR faults (Fig. 6) confirming that only a portion of such

789 faults ruptured during the sequence, without the rupture reaching the surface.
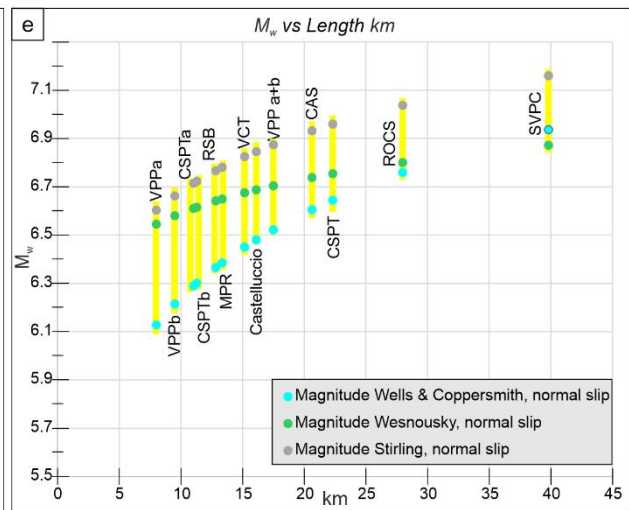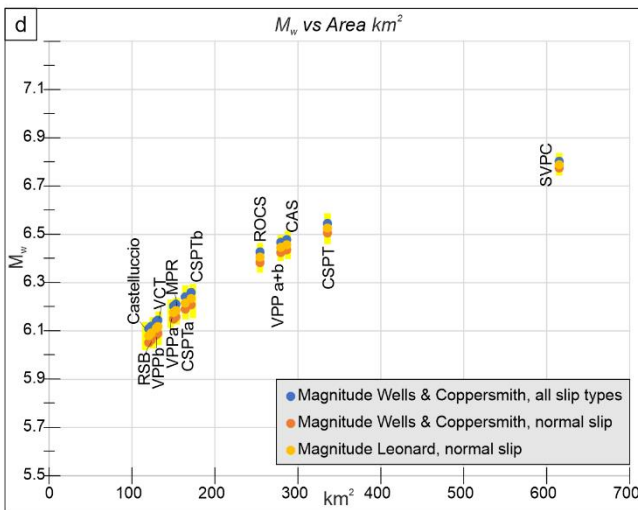
790

a Seismotectonic 3D Fault Model

Pollino Fault Barriers
CVN & POL

move

5km

b Surface projection of the modeled west dipping sources

CPTI 15 EQS
- 4.5<Mw<5.0 (green)
- 5.0<Mw<5.5 (yellow)
- 5.5<Mw<6.0 (orange)

2010-2018 EQS
- Mainshocks (red star)

Epicenters
- 1.0<Mw<5.2

1998 — 5.6
1980 — 4.1
1988 — 4.7
5.0 1894
1708 — 5.6
2012 — 5.2
2014 — 4.3
2012
1693 — 5.3
1559 — 4.9

0 5 10 20 kilometers

c Scaling Relationships for Seismic-Hazard Analysis

Fault Acronym	Area km²	Mw(a)	Mw(b)	Mw(c)	Length km	Mw(d)	Mw(e)	Mw(f)
VCT (1)	131.07	6.1	6.2	6.1	15.16	6.5	6.7	6.8
RSB (2)	123.39	6.1	6.1	6.1	12.82	6.4	6.7	6.8
ROCS (RSB + VCT)	254.46	6.4	6.4	6.4	27.98	6.8	6.8	7.0
MPR (3)	153.01	6.2	6.2	6.2	13.33	6.4	6.7	6.8
CAS (4)	286.49	6.5	6.5	6.4	20.64	6.6	6.7	6.9
Castelluccio (5)	120.35	6.1	6.1	6.1	16.12	6.5	6.7	6.9
CSPTa (6)	164.35	6.2	6.2	6.2	11.04	6.3	6.6	6.7
CSPTb (7)	171.33	6.2	6.3	6.2	11.28	6.3	6.6	6.7
CSPT a+b	335.68	6.5	6.6	6.5	22.32	6.6	6.8	7.0
VPPa (8)	150.06	6.2	6.2	6.2	8.00	6.1	6.5	6.6
VPPb (9)	129.28	6.1	6.1	6.1	9.49	6.2	6.6	6.7
VPP a+b	279.34	6.5	6.5	6.4	17.50	6.5	6.7	6.9
SPVC (VPP+CSPT)	615.02	6.8	6.8	6.8	39.81	6.9	6.9	7.2

a Leonard 2010 (Area), dip slip
$$M_w = 4.00 + \log A$$

b Wells & Coppersmith 1994 (Area), all slip types
$$M_w = 4.07 + 0.98 \log A$$

c Wells & Copp. 1994 (Area), normal slip
$$M_w = 3.93 + 1.02 \log A$$

d Wells & Copp. 1994 (Length), normal slip
$$M_w = 5.08 + 1.16 \log L$$

e Wesnousky 2008 (Length), normal slip
$$M_w = 6.12 + 0.47 \log L$$

f Stirling et. al. 2013 (Length), normal slip
$$M_w = 5.88 + 0.88 \log L$$

d M_w vs Area km²

Legend:
- Magnitude Wells & Coppersmith, all slip types
- Magnitude Wells & Coppersmith, normal slip
- Magnitude Leonard, normal slip

e M_w vs Length km

Legend:
- Magnitude Wells & Coppersmith, normal slip
- Magnitude Wesnousky, normal slip
- Magnitude Stirling, normal slip

791

Figure 9: (a) Seismotectonic 3D Fault Model in map view. (b) Box representation ~~of the 3D seismotectonic model~~ of the West-dipping seismogenic faults belonging to the 3DFM ~~in its~~ with detailed segmentation pattern. Fault traces are numbered according to the table of panel (c). ~~The~~ The associated historical earthquakes from CPTI15 v3.0 (4.5<M_w<6.0; Rovida et al., 2020, 2021) and the epicentral distribution of the 2010-2018 seismic activity occurred in the Pollino area (1.0<M_w<5.2) are also reported. (c) ~~Maximum e~~Expected magnitude according to scaling laws (Wells & Coppersmith 1994, Wesnousky 2008, Leonard 2010, Stirling et al. 2013) and calculated based on fault area (A) and length (L) ~~of each fault~~. (d-e) comparison of magnitude values calculated, for all the investigated active faults, using ~~Graph showing f~~Fault- area- (d) and f~~F~~ault length-(e) based~~based~~ scaling relationships. ~~(e) Fault length based scaling relationships comparing the values determined for all the investigated active normal faults and using six different empirical relations reported in panel (e).~~

6 Discussion

~~5~~6.~~2~~1 Seismogenic patches activated during 2010-2014 ~~seismic sequence~~

~~An attempt to reconstruct the seismogenic patches activated on the ROCS and MPR faults during 2010-2014 seismic sequence, is shown in Fig. 10. The~~ The seismogenic patches activated on the ROCS and MPR faults during the 2010-2014 seismic sequence~~,~~ are considered as the reasonable approximation of the actual portion of the faults which broke during the mainshock and the sequence of the early aftershocks. We obtained them by projecting the relocated hypocenters on the reconstructed fault surface and depicting their distribution using the Kernel density geostatistical analyst, available as a tool of the ESRI ArcGIS software package.~~patches can be considered the reasonable approximation of the actual portion of the faults which broke during the mainshock and the sequence of the early aftershocks.~~ The delimitation of each seismogenic patch and its ~~subsequent~~ parameterization allowed us ~~us~~ to verify ~~if there is a direct~~the correlation between its dimensions and the magnitude released by each fault during the mainshocks.

~~Operationally, we obtained the boundaries of the patches by projecting the relocated hypocenters on the reconstructed fault surface and depicting their distribution using the Kernel density geostatistical analyst, available as a tool of the ESRI ArcGIS software package.~~
~~At the depth at which the hypocenters of the 2010-2014 seismicity concentrate, the two segments of the W-dipping ROCS fault set, can be considered joined to form a single structure, thus a unique seismogenic patch was reconstructed.~~
The temporal analysis of the sequence~~,~~ show~~s~~ed that their overall extent was already well defined within the first 72 hours after the major events. Anyhow, inside the surrounding volumes, some seismicity had started before the mainshock ~~and also~~and continued to persist constantly throughout the development of the entire sequence so that they include a percentage ≥ of 70% of the whole hypocenter~~s~~ locations.
~~The delimitation of each seismogenic patch and its subsequent parameterization allowed us to verify if there is a direct correlation between its dimensions and the magnitude released by each fault during the mainshocks.~~

40

827   The along-strike elongation and area extent of the patches obtained over the VCT and MPR fault surfaces correspond to the

828   violet contoured area shown in Fig. 10. Their along-strike elongation and area extent can be assumed respectively as the

829   effective Subsurface Rupture Length and Rupture Area (RLD and RA in Fig. 10b, and 10c, respectively, according to Wells

830   and Coppersmith, 1994) associated with the M_w 5.2 Mormanno (on VCT fault) and M_w 4.0 and 4.3 Morano Calabro (on MPR

831   fault) earthquakes.

832   The parameters obtained for the VCT fault are RLD= 4.9 km and RA= 8.3 km^2. The values of, while RLD= 1.2 km and RA=

833   3.6 km^2 are assessed for the MPR fault.

834   Introducing the aforesaid parameters in the appropriate scale relationships (Fig. 10b,c) we observe a good agreement, or a

835   slight overestimation, between the theoretical magnitudes based on the Subsurface Rupture Length and the magnitudes of the

836   mainshocks. The values obtained for the VCT fault (causative of the M_w 5.2 Mormanno earthquake) are = M_w 5.3 whereas for

837   the MPR fault (causative of the M_w 4.0 and 4.3 Morano Calabro earthquakes) is M_w=4.5.

838   The magnitude calculated using the RA-based relationships provides values slightly lower than expected for the VCT

839   (4.9<M_w<5.0) and little slightly higher for the MPR (4.5<M_w<4.6).

840   In both cases, however, the magnitude values obtained using the scale relationships differ from those observed by an amount

841   <0.3.

842
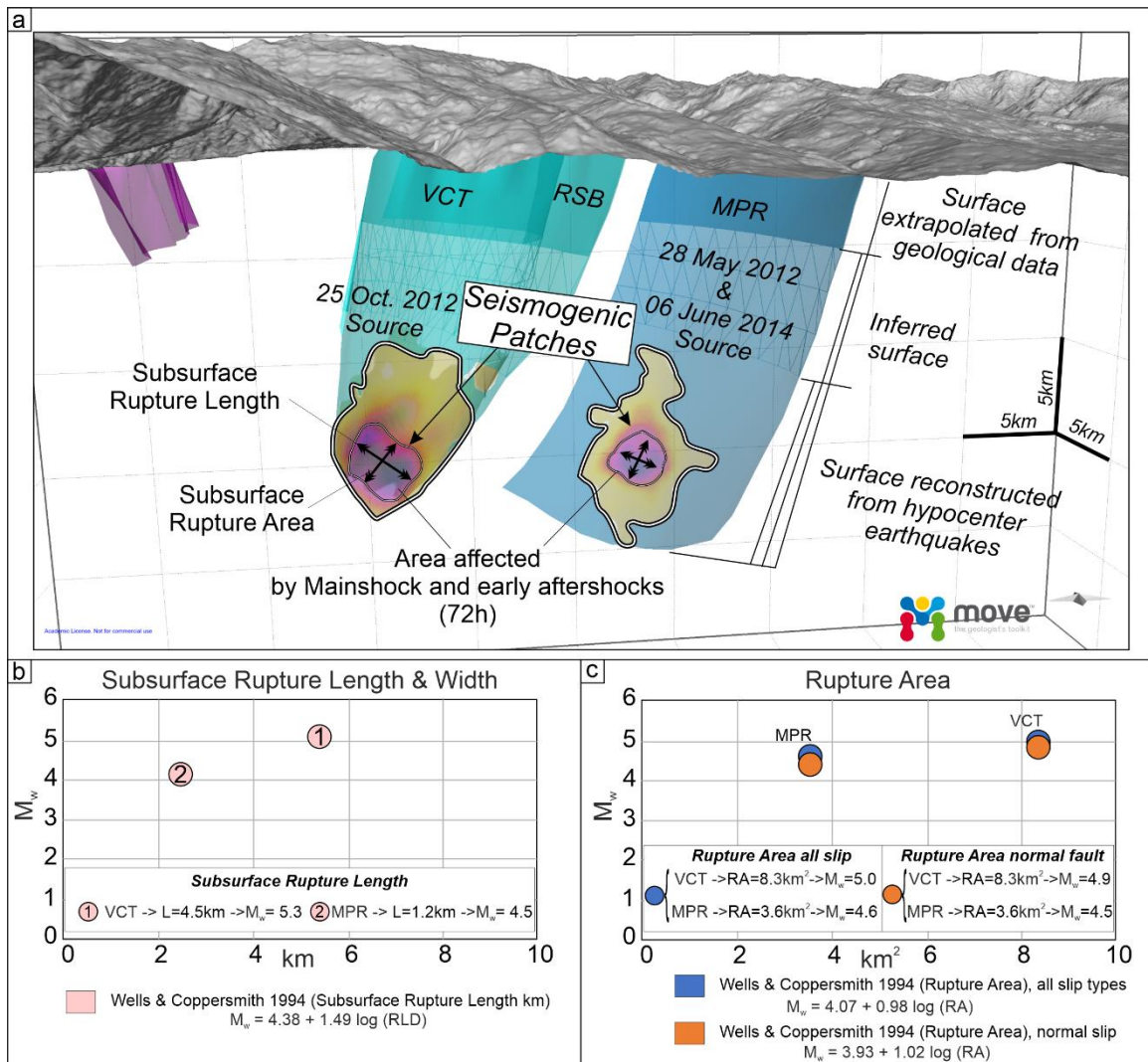
843
844
845 **Figure 10:** (a) Seismogenic patches activated during the 2010-2014 seismic ~~sequence~~ activity on VCT and MPR faults. The~~ir~~
846 along-strike elongation and area extent, shown by black arrows, are assumed to be the effective subsurface rupture length and
847 rupture area (RLD and RA, according to Wells and Coppersmith, 1994). The ~~associate~~dion of the patches' rupture with the
848 M_w 5.2 Mormanno of the 25 october 2012 (on VCT fault) and M_w 4.~~0~~3 and 4.~~3~~0 Morano Calabro (on MPR fault, 28 may
849 2012 and 6 june 2014 respectively) earthquakes is suggested~~, respectively~~. (b) and (c) show the RLD and RA, respectively,
850 obtained for both the VCT and MPR faults. ~~A comparison between the theoretical magnitudes (obtainable with scale~~
851 ~~relationships) based on the subsurface rupture length and the magnitudes of the mainshocks are also shown.~~.

852

853 ~~5~~6.~~3~~2 **Possible geometric restraints to coseismic rupture propagation**

854

42

855 The seismological dataset we used, demonstrates that the two main clusters of earthquakes of the 2010-2018 seismicity were

856 generated by as many independent sources related to the sub-parallel, 10 to 15 km-long, ROCS and MPR faults.

857 Brozzetti et al. (2017a) highlighted that the above seismogenic style, characterized by a perpendicular-to-fault strike evolution

858 of the seismic activity, is unlike from those which followed the major instrumental earthquakes recorded in the Apennine

859 Extensional Belt of Italy in recent years, such as the Colfiorito 1997 (M_w 6.0), L'Aquila 2009 (M_w 6.3) and Norcia 2016 (M_w

860 6.5) events (Chiaraluce et al. 2011, 2017; Lavecchia et al., 2011, 2012a, 2016). They also speculated that this peculiar

861 behaviour ~~of the 2010-2014 Pollino seismic sequence~~ could have been controlled by the geometric fault pattern of the area,

862 which is characterized by WSW-dipping ~~seismogenic~~ faults bounded southward by nearly E-W pre-existing structures. These

863 latter ~~which~~ are genetically related to the regional-scale, long-lived, "Pollino lineament" *s.l.*" (Bousquet, 1969, 1971; Ghisetti

864 and Vezzani, 1982, 1983; Knott and Turco, 1991; Van Dijk et al., 2000) and determine the abrupt contact between the Apennine

865 carbonate platform unit and the San Donato metamorphic core complex (Grandjaquet 1962; Servizio Geologico Nazionale,

866 1970; Amodio Morelli 1976). The cross-cut relationships detected in the field between the ROCS-MPR set and POL-CVN,

867 highlighted in our 3D model ~~(Fig. 8d)~~, lead us to exclude the latter fault to have a present seismogenic role, as also supported

868 by the distribution of the instrumental earthquakes which clusterized along with N-S-striking crustal volumes.

869 However, ~~it cannot be excluded that~~ this significant structural-geological boundary, ~~likely~~could exerts an influence on the

870 southward propagation of the ~~presently~~ currently active seismogenic faults, driving the eastward transfer of the active

871 extensional deformation belt. This inference is confirmed by the spatial distribution of the hypocentres of the whole 2010-

872 2018 relocated seismicity which, ~~with sporadic exceptions,~~ is confined within the CVN footwall (Fig. 8d).

873

874 ~~6~~ 7 Conclusions

875

876 We reconstructed in detail the 3D geometry and kinematics of the interconnected fault pattern responsible for the moderate-

877 magnitude earthquakes which recently affected the Pollino area (Calabrian-Lucanian boundary).

878 The main original outcomes ~~that we have achieved~~ are summarized as follows:

879 - ~~We computed t~~The geological and seismological stress tensors computed using geological- and seismological data and

880 demonstrated that they are consistent with a uniform normal faulting regime characterized by an ENE-WSW trending, sub-

881 horizontal σ3. This result confirms the coherence between the long-term and the present-day stress field and the persistence of

882 this extensional regime at least since the Middle Pleistocene.

883

884 - The 2010-2018 seismic activity which affected the study area followed a peculiar evolution ~~over time~~ characterized by the

885 concentration of epicenters in a series of sub-parallel ~NNW-SSE elongated clusters, independent and unconnected, which

886 can be related to two major near coaxial WSW-dipping faults possibly splaying from a common east-dipping basal detachment

887 and ~~almost~~ concurrently releasing seismicity.

888

889 - The accurate hypocenter re-locations~~, obtained by applying the non-linear Bayloc earthquake location algorithm, followed~~
890 ~~by the double-difference relative location method HypoDD, and using a 3D P-wave velocity model,~~ provided a ~~high-resolution~~
891 seismological dataset~~. The latter~~ that was ~~found to be of excellent quality for the purposes of 3D modelling. The correlation~~
892 correlated ~~between the~~with ~~geometry of the~~the active faults mapped at the surface~~,~~. The hypocenter spatial analysis ~~at the~~
893 ~~surface, and the distribution of seismicity at depth,~~ ~~allowed~~ allowing ~~us~~ to reconstruct the ~~3D~~ geometry (3DFM) of the
894 seismogenic sources which released seismicity during the 2010-201~~48 seismicity, and through~~ 2018. This reconstruction,
895 extrapolated down to the depth of ~10-12 km was the interpretative key to obtain the overall model of the Quaternary and
896 active ~~fault system~~extension in ~~of~~ the northern Calabria-Lucania Apennines~~, extrapolated down to the depth of ~10-12 km~~.
897 The 3DFM model includes all the faults playing a significant role, (either direct or indirect), on the seismogenesis of the study
898 area.
899
900 ~~- Our reconstruction~~We ~~confirms~~find ~~that t~~The western segment of the Pollino Fault (CVN), despite not being ~~pres~~currently
901 active, seems to maintain a significant seismotectonic role. In fact, juxtaposing crustal sectors with different structure and
902 composition (Apennine platform domain to the north, and San Donato metamorphic core to the south) may ~~acts~~ as a barrier to
903 the southern propagation of the seismogenic faults of the Mercure-Campotenese sector (ROCS, MPR), limiting their
904 dimensions and seismogenic potential.
905
906 - Based on the dimension and shape of all the active faults of the Pollino area,~~the seismogenic patches,~~ we ~~calculated~~obtained
907 ~~an~~ estimate~~d~~ ~~of~~ the ~~maximum~~ expected magnitudes ~~has been calculated~~ using appropriate scaling relationships~~, for all the~~
908 ~~active faults of the Pollino area~~. The complete rupture of individual W-dipping faults which are recognized to have been
909 causative of the 2010-2014 seismic ~~sequence~~activity ~~are~~ is expected to release a magnitude of ~M_w= 6.1 for the VCT and the
910 RSB, and of ~M_w= 6.2 for the MPR.~~-~~ Higher values, up to M_w=6.4, could be reached in the case of the complete and concurrent
911 rupture on both RSB and VCT. The ~~obtained~~ estimated values exceed the magnitudes of the associate earthquakes which struck
912 the area to date, ~~implying~~leading to hypothesize that the aforesaid faults released only partially their seismogenic potential.
913
914 - The delimitation of the fault patches ~~broken during the~~involved during 2010-2014 ~~seismic sequence~~, and their geometrical
915 parameterization, ~~allowed us to verify~~suggestsupport ~~that a high~~the consistenc~~y occurs~~ between the theoretical magnitudes
916 based on the Subsurface Rupture Length and the magnitudes of the mainshocks.
917 The estimates provided, for the VCT fault (which released the M_w 5.2 Mormanno earthquake) a ~~M_w~~M_w=5.3~~,~~ and~~,~~ for the MPR
918 fault (which released the M_w 4.0 and 4.3 Morano Calabro earthquakes)~~,~~ a M_w=4.5. The magnitudes calculated using the
919 relationships based on the Subsurface Rupture Area (~~4.9<M_w~<~~5.0 for the VCT and ~~4.5<M_w~<~~4.6 for the MPR), ~~instead~~
920 ~~deviate more~~show slightly greater deviation from the observed values.
921

44

~~- Our reconstruction confirms that the western segment of the Pollino Fault, despite not being presently active, seems to maintain a significant seismotectonic role. In fact, juxtaposing crustal sectors with different structure and composition (Apennine platform domain to the north, and San Donato metamorphic core to the south) acts as a barrier to the southern propagation of the seismogenic faults of the Mercure-Campotenese sector (ROCS, MPR), limiting their dimensions and seismogenic potential.~~

~~In conclusion, we want to~~We~~This study pointed out ~~that~~ as also even in the case of ~~moderate to minor~~low-to-moderate seismic ~~sequences~~activity, ~~as ~~like the Pollino 2010-2014 one, the approach based on the three-dimensional reconstruction of the ~~directly involved, as well as neighboring, ~~Quaternary fault surfaces (both directly involved and neighboring in the extensional system), represents a real breakthrough in the seismotectonic analysis and, ultimately, in the cognitive path that leads to a better assessment of the seismic hazard of a~~n~~ tectonically active area.

45

956

References

Allmendinger, R. W., Cardozo, N., and Fisher, D.: Structural geology algorithms: Vectors and tensors in structural geology: Cambridge University Press (book to be published in early 2012) 2012.

Amicucci, L., Barchi, M.R., Montone, P., and Rubilani, N.: The Vallo di Diano and Auletta extensional basins in the southern Apennines (Italy): a simple model for a complex setting, Terra Nova, 20, 475-482, https://doi.org/10.1111/j.1365-3121.2008.00841.x, 2008.

Amodio Morelli, L., Bonardi, G., Colonna, V., Dietrich, D., Giunta, G., Ippolito, F., Liguori, V., Lorenzoni, S., Paglionico, A., Perrone, V., Piccarreta, G., Russo, M., Scandone, P., Zanettin-Lorenzoni, E., and Zuppetta, A.: L'Arco calabro peloritano nell'orogene appenninico-maghrebide, Mem. Soc. Geol. It. 17, 1-60, 1976.

Angelier, J., and Mechler, ~~P.:~~P. : Sur une méthode graphique de recherche des contraintes principales également utilisable en tectonique et en séismologie: la méthode des dièdres droits, B. Soc. Gèol. Fr., 7, 1309–1318, 1977.

Arrigo, G., Roumelioti, Z., Benetatos, C., Kiratzi, A., Bottari, A., Neri, G., Termini, D., Gorini, A., and Marcucci, ~~S.:~~S. : A source study of the 9 September 1998 (Mw 5.6) Castelluccio Earthquakes in Southern Italy using Teleseismic and strong motion data, Nat. Hazards 00, 1-16, doi:10.1007/s1001 1069-1005-4644-1001, 2005.

Ascione, A., Mazzoli, S., Petrosino, P., and Valente, E.: A decoupled kinematic model for active normal faults: insights from the 1980, MS=6.9 Irpinia earthquake, southern Italy, GSA Bull 125, 1239-1259, doi:10.1130/B30814.1, 2013.

Barchi, M. R., De Feyter, A., Magnani, M. B., Minelli, G., Pialli, G., and Sotera, B. M.: Extensional tectonics in the northern Apennines (Italy): Evidence from the CROP03 deep seismic reflection line, Mem. Soc. Geol. Ital., 52, 527– 538, 1998.

990 Barchi, M., Lavecchia, G., Galadini, F., Messina, P., Michetti, A. M., Peruzza, L., Pizzi, A., Tondi, E., and Vittori, E.: Sintesi
991 delle conoscenze geologiche sulle faglie responsabili dei terremoti maggiori in Italia Centrale: Parametrizzazione ai fini della
992 caratterizzazione della pericolosità sismica, Gruppo Naz. per la Difesa dai Terremoti, CNR, Rome, 1999.

993

994 Barchi, M., Amato, A., Cippitelli, G., Merlini, S., and Montone, P.: Extensional tectonics and seismicity in the axial zone of
995 the southern Apennines, Boll. Soc. Geol. It. (Ital. J. Geosci.) 7, 47-56, 2007.

996

997 Bello S., de Nardis R., Scarpa R., Brozzetti F., Cirillo D., Ferrarini F., di Lieto B., Arrowsmith R. J., and Lavecchia G.: Fault
998 Pattern and Seismotectonic Style of the Campania-Lucania 1980 Earthquake (Mw 6.9, Southern Italy): New Multidisciplinary
999 Constraints, Frontiers in Earth Science, 8, 652, https://doi.org/10.3389/feart.2020.608063, 2021a.

1000

1001 Bello, S., Scott, C. P., Ferrarini, F., Brozzetti, F., Scott, T., Cirillo, D., de Nardis R., Arrowsmith R. J., and Lavecchia G.:
1002 High-resolution surface faulting from the 1983 Idaho Lost River Fault Mw 6.9 earthquake and previous events. Sci. Data 8,
1003 68, 1-20, https://doi.org/10.1038/s41597-021-00838-6, 2021b.

1004

1005 Bello, S., Andrenacci, C., Cirillo, D., Scott, T., Brozzetti, F., Arrowsmith R. J., and Lavecchia G.: High-detail fault
1006 segmentation: Deep insight into the anatomy of the 1983 Borah Peak earthquake rupture zone (Mw 6.9, Idaho, USA),
1007 Lithosphere, 2021c.

1008

1009 Blumetti, A. M., Esposito, E., Ferreli, L., Michetti, A. M., Porfido, S., Serva, L., et al.: New data and the reinterpretation of
1010 the ~~november~~ November 23, 1980, M 6.9, Irpinia-Lucania earthquake (Southern Apennines) coseismic surface effects, Spec.
1011 Issue Studi Geologici Camerti 2, 19-27, 2002.

1012

1013 Bousquet, J.C., and Gueremy, ~~P.:~~P. : Quelques Phénomènes de Néotectonique dans l'Apennin Calabro-Lucanien et Leurs
1014 Conséquences Morphologiques. Rev. Géogr. Phys. Géol. Dynam 10, 225-238, 1969.

1015

1016 Bousquet, ~~J.C.:~~J.C.-: La tectonique tangentielle des series calcareo-dolomitiques du ~~nord est~~nord-est de ~~l'apennin~~ l'Apennin
1017 Calabro-Lucanien (Italie Méridionale). Geol. Rom. X, 23-52, 1971.

1018

1019 Brozzetti, F., and Lavecchia, G.: Seismicity and related extensional stress field: the case of the Norcia Seismic Zone (Central
1020 Italy), Ann. Tectonicae, 8(1), 36-57, 1994.

1021

Brozzetti, F., Lavecchia, G., Mancini, G., Milana G. and Cardinali, M.: Analysis of the 9 September 1998 Mw 5.6 Mercure earthquake sequence (southern Apennines, Italy): a multidisciplinary approach, Tectonophysics, 476, 210-225. https://doi.org/10.1016/j.tecto.2008.12.007, 2009.

Brozzetti, F.: The Campania-Lucania extensional fault system (southern Italy): a suggestion for a uniform model of active extension in the Italian Apennines, Tectonics, 30 (5), 1-26, TC5009, http://dx.doi.org/10.1029/2010TC002794, 2011.

Brozzetti, F., Cirillo, D., Liberi, F., Faraca, E. and Piluso, E.: The Crati Valley Extensional System: field and subsurface evidences., Rend. Online Soc. Geol. It., Vol. 21 (2012), pp. 159-161.

Brozzetti, F., Cirillo, D., de Nardis, R., Cardinali, M., Lavecchia, G., Orecchio, B., Presti D., and Totaro, C.: Newly identified active faults in the Pollino seismic gap, southern Italy, and their seismotectonic significance, J. Struct. Geol., 94, 13-31, https://doi.org/10.1016/j.jsg.2016.10.005, 2017a.

Brozzetti, F., Cirillo, D., Liberi, F., Piluso, E., Faraca, E., De Nardis, R., and Lavecchia, G.: Structural style of Quaternary extension in the Crati Valley (Calabrian Arc): Evidence in support of an east-dipping detachment fault, It. Journ. of Geosci., 136(3), 434-453, https://doi.org/10.3301/IJG.2017.11, 2017b.

Brozzetti, F., Cirillo, D., and Luchetti, L.: Timing of Contractional Tectonics in the Miocene Foreland Basin System of the Umbria Pre-Apennines (Italy): An Updated Overview, Geosciences 2021, 11, 97. https://doi.org/10.3390/geosciences11020097, 2021.

Caiazzo, C., Giovine, B., Ortolani, F., Pagliuca, S., Schiattarella, M., andbBarchi and Vitale, C. : Genesi ed evoluzione strutturale della depressione tettonica dell'alta valle del Fiume Sele (Appennino Campano Lucano), Stud. Geol. Camerti, 1992(1), 245–255, 1992.

Calamita, F., Pizzi, A., and Roscioni, M.: I fasci di faglie recenti ed attive di M. Vettore - M. Bove e di M. Castello - M. Cardosa (Appennino Umbro-Marchigiano), In Studi Geologici Camerti; Università di Camerino: Camerino, Italy, 81-95, 1992; Available online: http://193.204.8.201:8080/jspui/handle/1336/552, last access: 19 April 2021.

Castaldo, R., de Nardis, R., De Novellis, V., Ferrarini, F., Lanari, R., Lavecchia, G., et al.: Coseismic stress and strain field changes investigation through 3-D Finite Element modeling of DInSAR and GPS measurements and geological/seismological data: the l'aquila (Italy) 2009 earthquake case study, J. Geophys. Res. Solid Earth 123, 4193-4222, https://doi.org/10.1002/2017JB014453, 2018.

1056

1057   Castello, B., Selvaggi, G., Chiarabba, C., and Amato, A.: CSI Catalogo della sismicità italiana 1981-2002, versione 1.1. Roma:

1058   INGV-CNT, 2006, https://csi.rm.ingv.it/, last access: 19 April 2021.

1059

1060   Cello, G., Tondi, E., Micarelli, L., and Mattioni L.: Active tectonics and earthquake sources in the epicentral area of the 1857

1061   Basilicata earthquake (southern Italy), Journal of Geodynamics, 36, 1-2, 37-50, https://doi.org/10.1016/S0264-3707(03)00037-

1062   1, 2003.

1063

1064   Cheloni, D., D'Agostino, N., Selvaggi, G., Avallone, A., Fornaro, G., Giuliani, R., Reale, D., Sansosti, E., and Tizzani, P.,:

1065   Aseismic transient during the 2010–2014 seismic swarm: evidence for longer recurrence of Ml $\geq$6.5 earthquakes in the Pollino

1066   gap (Southern Italy)?, Sci. Rep., 7(576), https://doi.org/10.1038/s41598-017-00649-z, 2017.

1067

1068   Chiaraluce, L., Amato, A., Cocco, M., Chiarabba, C., Selvaggi, G., Di Bona, M., Piccinini, D., Deschamps, A., Margheriti, L.,

1069   Courboulex, F., and Ripepe, M.: Complex normal faulting in the Apennines thrust-and-fold belt: The 1997 seismic sequence

1070   in Central Italy, Bull. Seismol. Soc. Am. 94, 99-116, https://doi.org/10.1785/0120020052, 2004.

1071

1072   Chiaraluce, L., Barchi, M.R., Collettini, C., Mirabella, F., and Pucci, S.: Connecting seismically active normal faults with

1073   Quaternary geological structures: the Colfiorito 1997 case history (Northern Apennines, Italy), Tectonics 24, TC1002, 1-16,

1074   https://doi.org/10.1029/2004TC001627, 2005.

1075

1076   Chiaraluce, L., Valoroso, L., Piccinini, D., Di Stefano, R., and De Gori, P.: The anatomy of the 2009 L'Aquila normal fault

1077   system (central Italy) imaged by high resolution foreshock and aftershock locations, J. Geophys. Res. 116, no. B12,

1078   https://doi.org/10.1029/2011JB008352, 2011.

1079

1080   Chiaraluce, L., Di Stefano, R., Tinti, E., Scognamiglio, L., Michele, M., Casarotti, E., Cattaneo, M., De Gori, P., Chiarabba,

1081   C., Monachesi, G., Lombardi, A., Valoroso, L., Latorre, D., and Marzorati, S.: The 2016 Central Italy Seismic Sequence: A

1082   First Look at the Mainshocks, Aftershocks, and Source Models, Seismological Research Letters, 88(3), 757-771,

1083   https://doi.org/10.1785/0220160221, 2017.

1084

1085   Cinque, A., Patacca, E., Scandone, P., and Tozzi, M.: Quaternary kinematic evolution of the southern apennines. relationship

1086   between surface geological features and lithospheric structures, Ann. Geofisc 36, 249–260. https://doi.org/10.4401/ag-4283,

1087   1993.

1088

Cinque, A., Ascione, A., and Caiazzo, C.: Distribuzione spaziotemporale e caratterizzazione della fagliazione quaternaria in Appennino meridionale, in Le Ricerche del GNDT nel Campo Della Pericolosità Sismica (1996–1999), edited by F. Galadini, C. Meletti, and A. Rebez, 397 pp., CNR, Gruppo Naz. per la Difesa dai Terremoti, Rome, 2000.

Cinti, F. R., Cucci, L., Pantosti, D., D'Addezio, G., and Meghraoui, M.: A major seismogenic fault in a 'silent area': the Castrovillari fault (southern Southern Apennines, Italy), Geophysical Journal International, 130(3), 595-605, 1997. https://www.earth-prints.org/bitstream/2122/12031/1/text.pdf, last access: 19 April 2021.

Cinti, F. R., Moro, M., Pantosti, D., Cucci, L., and D'Addezio, G.: New constraints on the seismic history of the Castrovillari fault in the Pollino gap (Calabria, southern Italy), J. Seismol., 6, 199-217. https://doi.org/10.1023/A:1015693127008, 2002.

Cirillo, D.: Digital Field Mapping and Drone-Aided Survey for Structural Geological Data Collection and Seismic Hazard Assessment: Case of the 2016 Central Italy Earthquakes, Applied Sciences, 10, 5233. https://doi.org/10.3390/app10155233, 2020.

D'Agostino, N.: Complete seismic release of tectonic strain and earthquake recurrence in the Apennines (Italy), Geophys. Res. Lett 41, 1155-1162, https://doi.org/10.1002/2014GL059230, 2014.

D'Alessandro, A., Gervasi, A., and Guerra, I.: Evolution and strengthening of the Calabrian regional seismic network. Adv. Geosciences 36, 11-16, 2013. https://adgeo.copernicus.org/articles/36/11/2013/adgeo-36-11-2013.pdf, last access: 19 April 2021.

D'Argenio, B.: L'Appennino Campano Lucano. Vecchi e nuovi modelli geologici tra gli anni sessanta e gli inizi degli anni ottanta. Mem. Soc. Geol. It. 41, 3-15, 1992.

Delaunay, B.: Sur la sphere vide, Bull. Acad. Sci. USSR(VII), Classe Sci. Mat. Nat., 793-800, 1934.

Delvaux, D., and Sperner, B.: New aspects of tectonic stress inversion with reference to the TENSOR program. In: New Insights into Structural Interpretation and Modelling (D.A. Nieuwland, ed.), J. Geol. Soc. London Spec. Publ., 212, 75-100, 2003.

Delvaux, D., and Barth, A.: African stress pattern from formal inversion of focal mechanism data, Tectonophysics, 482, 105-128, 2010.

Di Bucci, D., Buttinelli, M., D'Ambrogi, C., and Scrocca, D., and the RETRACE-3D Working Group: The RETRACE-3D multi-data and multi-expertise approach towards the construction of a 3D crustal model for the 2016-2018 Central Italy seismic sequence, Boll. Geof. Teor. Appl. DOI 10.4430/bgta0343, 2021.

Elter, P., Giglia, G., Tongiorgi, M., and L. Trevisan, L.: Tensional and compressional areas in the recent (Tortonian to present) evolution of the northern Apennines, Boll. Geofis. Teor. Appl., 17, 3-18, 1975.

Ercoli, M., Pauselli, C., Forte, E., Frigeri, A., and Federico, C.: The Mt. Pollino Fault (southern Apennines, Italy): GPR signature of Holocenic earthquakes in a "silent" area. In: Advanced Ground Penetrating Radar (IWAGPR), 2013 7th International Workshop. IEEE, pp. 1-6. http://dx.doi.org/10.1109/IWAGPR.2013.6601510, 2013.

Ercoli, M., Cirillo, D., Pauselli, C., Jol, H. M., and Brozzetti, F.: GPR signature of Quaternary faulting: a study from the Mt. Pollino region, southern Apennines, Italy, Solid Earth, https://doi.org/10.5194/se-2021-75, 2021. Ercoli M., Cirillo D., Pauselli C., Jol H. M., and Brozzetti F.: GPR signature of Quaternary faulting: a study from the Mt. Pollino region, southern Apennines, Italy, submitted this special issue Solid Earth, 2021.

Faure Walker, J. P., Roberts, G. P., Cowie, P. A., Papanikolaou, I., Michetti, A. M., Sammonds, P., et al.: Relationship between topography, rates of extension and mantle dynamics in the actively-extending italianItalian apenninesApennines, Earth Planet Sci. Lett 325–326, 76–84. doi:10.1016/j.epsl.2012.01.028, 2012.

Ferranti, L., Milano, G., and Pierro, M., Insights on the seismotectonics of the western part of northern Calabria (southern Italy) by integrated geological and geophysical data: coexistence of shallow extensional and deep strike-slip kinematics, Tectonophysics, 721, 372–386, https://doi.org/10.1016/j.tecto.2017.09.020, 2017.

Ferrarini, F., Lavecchia, G., de Nardis, R., and Brozzetti, F.: Fault geometry and active stress from earthquakes and field geology data analysis: the Colfiorito 1997 and L'Aquila 2009 cases (central Italy), Pure Appl. Geoph., 172 (5), 1079-1103, https://doi.org/10.1007/s00024-014-0931-7, 2015.

Ferrarini, F., Boncio, P., de Nardis, R., Pappone, G., Cesarano, M., Aucelli, P.P.C., and Lavecchia, G.: Segmentation pattern and structural complexities in seismogenic extensional settings: The North Matese Fault System (Central Italy), J. Struct. Geol., 95, 93-112, http://dx.doi.org/10.1016/j.jsg.2016.11.006, 2017.

Ferrarini, F., de Nardis, R., Brozzetti, F., Cirillo, D., Arrowsmith, JR. and Lavecchia, G.: Multiple Lines of Evidence for a Potentially Seismogenic Fault Along the Central-Apennine (Italy) Active Extensional Belt–An Unexpected Outcome of the MW6.5 Norcia 2016 Earthquake, Front. Earth Sci. 9:642243. doi: 10.3389/feart.2021.642243, 2021.

Filice, F., Liberi, F., Cirillo, D., Pandolfi, L., Marroni, M., and Piluso E.: Geology map of the central area of Catena Costiera: insights into the tectono-metamorphic evolution of the Alpine belt in Northern Calabria, Journal of Maps, 11(1), 114-125, https://doi.org/10.1080/17445647.2014.944877, 2015.

Filice, F., and Seeber, L.: The Culmination of an Oblique Time-Transgressive Arc Continent Collision: The Pollino Massif Between Calabria and the Southern Apennines, Italy, Tectonics, 38(1), 3261-3280. https://doi.org/10.1029/2017TC004932, 2019.

Frepoli, A., Cinti, R., Amicucci, L., Cimini, G.B., De Gori, P., and Pierdominici, S.: Pattern of seismicity in the Lucanian Apennines and foredeep (Southern Apennines) from recording by SAPTEX temporary array, Annal. Geophys., 48, 1035-1054, 2005. https://www.earth-prints.org/bitstream/2122/1131/6/manuscript.pdf , last access: 19 April 2021.

Frohlich, C.: Display and quantitative assessment of distributions of earthquakes focal mechanisms, Geophys. J. Int. 144, 300-308, 2001.

Gafarov, K., Ercoli, M., Cirillo, D., Pauselli, C., and Brozzetti, F.: Extending surface geology data through GPR prospections: Quaternary faulting signature from the Campotenese area (Calabria-Italy), 17th International Conference on Ground Penetrating Radar, GPR, 8441611, 2018.

Galadini, F., and P. Galli: Active tectonics in the Central Apennines (Italy): Input data for seismic hazard assessment, Nat. Hazards, 22, 225–268, doi:10.1023/A:1008149531980, 2000.

Galli, P., and Peronace, E.: New paleoseismic data from the Irpinia fault. A different seismogenic perspective for the southern Apennines, Earth Sci. Rev. 136, 175-201, https://doi.org/10.1016/j.earscirev.2014.05.013, 2014.

Galli, P.: Recurrence times of central-southern Apennine faults (Italy): Hints from paleoseismology, Terra Nova, 32, 399-407, https://doi.org/10.1111/ter.12470, 2020.

Gephart, J.W., and Forsyth, D.W.: An improved method for determining the regional stress tensor using earthquake focal mechanism data: application to the San Fernando earthquake sequence, J. Geophys. Res., 89, 9305-9320, 1984.

1190

1191 Ghisetti, F., and Vezzani, L.: Strutture tensionali e compressive indotte da meccanismi profondi lungo la linea del Pollino

1192 (Appennino meridionale), Boll. Soc. Geol. It. 101, 385-440, 1982.

1193

1194 Ghisetti, F., and Vezzani, L.: Structural Map of Mt. Pollino (Southern Italy), 1:50.000 Scale, SELCA, Firenze,1983.

1195

1196 Giano, S. I., and Martino, C.: Assetto morfotettonico e morfostratigrafico di alcuni depositi continentali pleistocenici del bacino

1197 del ~~pergola~~Pergola ~~melandro~~ Melandro (Appennino Lucano). Quaternario 16 (2), 289–297, 2003.

1198

1199 Grandjacquet, C.: Données nouvelles sur la tectonique tertiaire des massif Calabro-Lucaniens. Bull. Soc. Geol. Fr. 7ème série

1200 4, 695-706, 1962.

1201

1202 Guerra, I., Harabaglia, P., Gervasi, A., and Rosa, A.B.: The 1998–1999 Pollino (Southern Apennines, Italy) seismic crisis:

1203 tomography of a sequence, Ann. Geophys. 48, 995-1007, https://doi.org/10.4401/ag-3249, 2005.

1204

1205 Guidoboni E., Ferrari G., Mariotti D., Comastri A., Tarabusi G., Sgattoni G., and Valensise G.: CFTI5Med, Catalogo dei Forti

1206 Terremoti in Italia (461 a.C.-1997) e nell'area Mediterranea (760 a.C.-1500), Istituto Nazionale di Geofisica e Vulcanologia

1207 (INGV), http://storing.ingv.it/cfti/cfti5/, 2018.

1208

1209 Guidoboni, E., Ferrari, G., Tarabusi, G., Sgattoni, G., Comastri, A., Mariotti, D., Ciuccarelli, C., Bianchi, M.G., and Valensise

1210 G.: CFTI5Med, the new release of the catalogue of strong earthquakes in Italy and in the Mediterranean area, Scientific Data

1211 6, ~~Article~~article number: 80, doi: https://doi.org/10.1038/s41597-019-0091-9, 2019.

1212

1213 Heidbach, O., Tingay, M., Barth, A., Reinecker, J., Kurfeß, D., and Müller, B.: Global crustal stress pattern based on the world

1214 stress map database release 2008, Tectonophysics 482, 3-15, https://doi.org/10.1016/j.tecto.2009.07.023, 2010.

1215

1216 Hippolite, J.C., Angelier, J., and Barrier, E.: Compressional and extensional tectonics in an arc system; example of the Southern

1217 Apennines, J. Struct. Geol. 17, 1725–1740, https://doi.org/10.1016/0191-8141(95)00066-M, 1995.

1218

1219 Husen, S., and Smith, R.: Probabilistic earthquake location in ~~three dimensional~~three-dimensional velocity models for the

1220 Yellowstone National Park region, Wyoming, Bull. Seism. Soc. Am. 94 (6), 880-896, 2004.

1221 https://uusatrg.utah.edu/PAPERS/husen2004probeqreloc.pdf, last access: 19 April 2021.

1222

1223 Iannace, A., D'Errico, M., and Vitale, S.: Carta Geologica dell'area compresa tra Maratea, Castrovillari e Sangineto. In: Vitale,
1224 S., Iannace, A. (Eds.), Analisi Dello Strain Finito in 3D Dell'Unità Pollino-Ciagola (Confine Calabro-lucano, Italia
1225 Meridionale), Studi Geologici Camerti, Nuova Serie, 2, 153-167 (ISSN: 0392-0631), 2004.

1227 Iannace, A., Garcia Tortosa, F.J., and Vitale, S.: The Triassic metasedimentary successions across the boundary between
1228 Southern Apennines and Calabria–Peloritani Arc (Northern Calabria, Italy), Geol. J., 40, 155–171.
1229 https://doi.org/10.1002/gj.1001, 2005.

1231 Iannace, A., Vitale, S., D'Errico, M., Mazzoli, S., Di Staso, A., Macaione, E., Messina, A., Reddy, S.M., Somma, R.,
1232 Zamparelli, V., Zattin, M., and Bonardi, G.: The carbonate tectonic units of northern Calabria (Italy): a record of Apulian
1233 palaeomargin evolution and Miocene convergence, continental crust subduction, and exhumation of HP–LT rocks, J. Geol.
1234 Soc. Lond. 164, 1165-1186. https://doi.org/10.1144/0016-76492007-017, 2007.

1236 Ietto, A., and Barilaro, A.M.: L'Unità di San Donato quale margine deformato Cretacico-Paleogene del bacino di Lagonegro
1237 (Appennino Meridionale-Arco Calabro), Boll. Soc. Geol. It. 112, 477-496, 1993.

1239 ISIDe Working Group: Italian Seismological Instrumental and Parametric Database (ISIDe). Istituto Nazionale di Geofisica e
1240 Vulcanologia (INGV), https://doi.org/10.13127/ISIDE, 2007, last access: 19 April 2021.

1242 Johnson, K., Nissen, E., Saripalli, S., Arrowsmith, J.R., McGarey, P., Scharer, K., Williams, P., Blisniuk, K.: Rapid mapping
1243 of ultrafine fault zone topography with structure from motion, Geosphere, 10, 969–986, 2014.

1245 Klin, P., Laurenzano, G., Romano, M.A., Priolo, E., Martelli, L.: ER3D: a structural and geophysical 3-D model of central 742
1246 Emilia-Romagna (northern Italy) for numerical simulation of earthquake ground motion, Solid Earth, 743, 10:931–949.
1247 https://doi.org/10.5194/se-10-931-2019. 2019.

1250 Knott, S.D., and Turco, E.: Late cenozoic kinematics of the Calabrian arc, southern Italy. Tectonics 10 (6), 1164-1172, 1991.

1252 Lavecchia, G., Brozzetti, F., Barchi, M., Menichetti, M., and Keller, J. V. A.: Seismotectonic zoning in east-central Italy
1253 deduced from an analysis of the ~~neogene~~ Neogene to present deformations and related stress fields, Geol. Soc. Am. Bull. 106,
1254 1170-1120, doi:10.1130/0016, https://doi.org/10.1130/0016-7606(1994)106%3C1107:SZIECI%3E2.3.CO;2, 1994.

1256 Lavecchia, G., Boncio, P., Brozzetti, F., De Nardis, R., Di Naccio, D., Ferrarini, F., Pizzi, A., and Pomposo, G.: The April

1257 2009 L'Aquila (central Italy) seismic sequence (Mw 6.3): a preliminary seismotectonic picture, Recent Prog. Earthquake Geol.

1258 2011, 1-17, ISBN: 978-1-60876-147-0, 2011.

1259

1260 Lavecchia, G., Ferrarini, F., Brozzetti, F., de Nardis, R., Boncio, P., and Chiaraluce, L.: From surface geology to aftershock

1261 analysis: constraints on the geometry of the L'Aquila 2009 seismogenic fault system. Italian J. Geosciences 131 (3), 330-347,

1262 2012a.

1263

1264 Lavecchia, G., de Nardis, R., Cirillo, D., Brozzetti, F., and Boncio, P.: The May-June 2012 Ferrara Arc earthquakes (northern

1265 Italy): structural control of the spatial evolution of the seismic sequence and of the surface pattern of coseismic fractures,

1266 Annals of Geophysics, 55, 4, doi: 10.4401/ag-6173, 2012b

1267

1268 Lavecchia G., de Nardis, R., Costa, G., Tiberi, L., Ferrarini, F., Cirillo, D., Brozzetti F., and Suhadolc, P.: Was the Mirandola

1269 thrust really involved in the Emilia 2012 seismic sequence (northern Italy)? Implications on the likelihood of triggered

1270 seismicity effects, Boll. Geof. Teor. Appl., Vol. 56, n. 4, pp. 461- 488, 2015.

1271

1272 Lavecchia, G., Castaldo, R., de Nardis, R., De Novellis, V., Ferrarini, F., Pepe, S., Brozzetti, F., Solaro, G., Cirillo, D., Bonano,

1273 M., Boncio, P., Casi, F., De Luca, C., Lanar, R., Manunta, M., Manzo, M., Pepe, A., Zinno, I., and Tizzani, P.: Ground

1274 deformation and source geometry of the 24 August 2016 Amatrice earthquake (Central Italy) investigated through analytical

1275 and numerical modeling of DInSAR measurements and structural-geological data, Geophys. Res. Lett., 43,

1276 https://doi.org/10.1002/2016GL071723, 2016

1277

1278 Lavecchia, G., Adinolfi, G. M., de Nardis, R., Ferrarini, F., Cirillo, D., Brozzetti, F., De Matteis, R., Festa, G., and Zollo, A.:

1279 Multidisciplinary inferences on a newly recognized active east-dipping extensional system in central Italy, Terra Nova, 29,

1280 77–89, https://doi.org/10.1111/ter.12251, 2017.

1281

1282 Lavecchia, G., de Nardis, R., Ferrarini, F., Cirillo, D., Bello, S., and Brozzetti, F.: Regional seismotectonic zonation of

1283 hydrocarbon fields in active thrust belts: a case study from Italy, in Building knowledge for geohazard assessment and

1284 management in the caucasus and other orogenic regions, Editors F. L. Bonali, F. Pasquaré Mariotto, and N. Tsereteli (the

1285 Netherlands: Springer), doi:10.1007/978-94-024-2046-3, 2021.

1286

1287 Leonard, M.: Earthquake fault scaling: Relating rupture length, width, average displacement, and moment release, Bull.

1288 Seismol. Soc. Am., 100(5A), 1971-1988. https://doi.org/10.1785/0120090189, 2010.

1289

Liberi, F., Morten, L., and Piluso, E.: Geodynamic significance of the ophiolites within the Calabrian Arc, Island Arc, 15, 26–43, https://doi.org/10.1111/j.1440-1738.2006.00520.x, 2006.

Liberi, F., and Piluso, E.: Tectonometamorphic evolution of the ophiolitic sequences from Northern Calabrian Arc, Italian Journal Geoscience (Boll.ettino Society Geological Italian), 128, 483–493, https://doi.org/10.3301/IJG.2009.128.2.483, 2009.

Lippmann-Provansal, M.:M. : L'Appennin meridionale (Italie): Etude geomorphologique, these Doctorat, Univ. d'AixD'Aix-Marseille II, Marseille, France, 1987.

Lomax, A., Virieux, J., Volant, P., and Berge-Thierry, C.: Probabilistic Earthquake Location in 3D and Layered Model, in Advances in Seismic Event Location, Pp. 101-134, Kluwer Academic Publishers, Netherlands, 2000.

Margheriti, L., Amato, A., Braun, T., Cecere, G., D'Ambrosio, C., De Gori, and P., Selvaggi, G.: Emergenza nell'area del Pollino: le attività della Rete Sismica Mobile, Rapporti Tecnici INGV, 2013.

Mariucci, M.T., and Montone, P.: Database of Italian present-day stress indicators, IPSI 1.4, Sci. Data 7, 298. https://doi.org/10.1038/s41597-020-00640-w, 2020.

Marrett, R. A., and Allmendinger, R. W.: Kinematic analysis of fault slip data, Journal of Structural Geology, v. 12, p. 973-986, 1990.

Maschio, L., Ferranti, L., and Burrato, P.: Active extension in Val d'Agri area, southern Apennines, Italy: Implications for the geometry of the seismogenic belt, Geophys. J. Int., 162, 591–609, https://doi.org/10.1111/j.1365-246X.2005.02597.x., 2005.

Michetti, A. M., Ferreli, L., Serva, L., and Vittori, E.: Geological evidence for strong historical earthquakes in an "aseismic" region: The Pollino case (Southern Italy), Journal of Geodynamics, 24:1-4, 67-86. https://doi.org/10.1016/S0264-3707(97)00018-5, 1997.

Michetti, A. M., Ferreli, L., Esposito, E., Porfido, S., Blumetti, A. M., Vittori, E., Serva, L., and Roberts, G. P.: Ground Effects during the 9 September 1998, Mw = 5.6 Lauria, Earthquake and the Seismic Potential of the seismic Pollino Region in Southern Italy, Seismological Research Letters, 71(1), 31-46. https://doi.org/10.1785/gssrl.71.1.31, 2000.

Montone, P., Mariucci, M.T., Pondrelli, S., Amato, A.: An improved stress map for Italy and surrounding regions (central Mediterranean), J. Geophys. Res. 109, B10410. http://dx.doi.org/10.410.11029/12003JB002703, 2004.

1324

1325 Montone, P., and Mariucci, M.T., and Pierdominici, S.: The New Release of the Italian Contemporary Stress Map, Geophys.

1326 J. Int., 205 (3), 1525–1531. https://doi.org/10.1093/gji/ggw100, 2016. The Italian present-day stress map, Geophys. J. Int., 189,

1327 705-716; https://doi.org/10.1111/j.1365-246X.2012.05391.x, 2012.

1328

1329 Mostardini, F., and Merlini, S.: Appennino centro meridionale - Sezioni geologiche e proposta di modello strutturale. Mem.

1330 Soc. Geol. Ital. 35, 177–202, 1986

1331

1332 Napolitano, F., De Siena, L., Gervasi, A., Guerra, I., Scarpa, R., and La Rocca, M.: Scattering and absorption imaging of a

1333 highly fractured fluid-filled seismogenetic volume in a region of slow deformation, Geosci. Front., 11(3), 989-998.

1334 https://doi.org/10.1016/j.gsf.2019.09.014, 2020.

1335

1336 Napolitano, F., Galluzzo, D., Gervasi, A., Scarpa, R., La Rocca, M.: Fault imaging at Mt Pollino (Italy) from relative location

1337 of microearthquakes, Geophysical Journal International, 224(1), 637-648, https://doi.org/10.1093/gji/ggaa407 , 2021.

1338

1339 Nicholson, G., Plesch, A., Sorlion, C. C., Shaw, J. H., and Hauksson, E.: TheSCEC 3D community fault model (CFM-v5): an

1340 updated and expanded fault set of oblique crustal deformation and complex fault interaction for southern California, Eos Trans.

1341 Am. Geophys. Union 95 (52). Abstract T31B-4584, 2014.

1342

1343 Nicholson, C., Plesch, A., Sorlien, C. C., Shaw, J. H., and Hauksson, E.: The SCEC community fault model version 5.0: an

1344 updated and expanded 3D fault set for southern California, in 2015 pacific section AAPG joint meeting program (Oxnard,

1345 CA), Vol. 77, September 12-16, 2015.

1346

1347 Ogniben, L.: Schema introduttivo alla geologia del confine calabro-lucano, Mem. Soc. Geol. It, 8, 453-763, 1969.

1348

1349 Ogniben, L.: Schema geologico della Calabria in base ai dati odierni, Geologia Romana, 12, 243–585, 1973.

1350

1351 Orecchio, B., Presti, D., Totaro, C., Guerra, I., and Neri, G.: Imaging the velocity structure of the Calabrian Arc region (south

1352 Italy) through the integration of different seismological data, Boll. Geofis. Teor. Appl. 52, 625-638, 2011,

1353 http://www3.ogs.trieste.it/bgta/pdf/bgta0023_ORECCHIO.pdf last access: 19 April 2021.

1354

1355 Pantosti, D., and Valensise, G.: Faulting mechanism and complexity of the november 23, 1980, campaniaCampania-lucania

1356 Lucania earthquake, inferred from surface observation, J. Geophys. Res 95, 15319. doi:10.1029/jb095ib10p15319, 1990.

1357

1358 Pantosti, D., and Valensise, G.: Source geometry and ~~long term~~long-term behavior of the 1980, Irpinia earthquake fault based
1359 on field geologic observations. Ann. Geofisc 36, 41–49. https://doi.org/10.4401/ag-4299, 1993.

1361 Papanikolaou, I. D., and Roberts, G. P.: Geometry, kinematics and deformation rates along the active normal fault system in
1362 the southern Apennines: implications for fault growth, J. Struct. Geol 29, 166-188. https://doi.org/10.1016/j.jsg.2006.07.009,
1363 2007.

1365 Passarelli, L., Hainzl, S., Cesca, S., Meccaferri, F., Mucciarelli, M., Roessler, D., Corbi, F., Dahm, T., and Rivalta, E.: Aseismic
1366 transient driving the swarm-like seismic sequence in the Pollino range, Southern Italy, Geophys. J. Int., 201(3), 1553–1567,
1367 https://doi.org/10.1093/gji/ggv111, 2015.

1369 Pastori, M., Margheriti, L., De Gori, P., Govoni, A., Lucente, F.P., Moretti, M., Marchetti, A., Di Giovambattista, R., Anselmi,
1370 M., De Luca, P., Nardi, A, Agostinetti, N.P., Latorre, D., Piccinini, D., Passarelli, L., and Chiarabba, C.: The 2011–2014
1371 Pollino Seismic Swarm: Complex Fault Systems, Imaged by 1D Refined Location and Shear Wave Splitting Analysis at the
1372 Apennines–Calabrian Arc Boundary, Front. Earth Sci. 9:618293. doi: 10.3389/feart.2021.618293, 2021.

1374 Patacca, E., and Scandone, P.: Geological interpretation of the CROP-04 seismic line (Southern Apennines, Italy), Boll. Soc.
1375 Geol. It. (Ital. J. Geosci.), 7, 297-315, 2007.

1377 Plesch, A., Shaw, J. H., and Jordan, T. H.: Stochastic descriptions of basin velocity structure from analyses of sonic logs and
1378 the SCEC community velocity model (CVM-H), in Presentation at 2014 SSA annual meeting, Palm Springs, CA, September
1379 6-10, 2014.

1381 Pondrelli, S., Salimbeni, S., Ekström, G., and Morelli, A.: The Italian CMT dataset from 1977 to the present, Phys. Earth
1382 Planet, In 159, 286–303, https://doi.org/10.1016/j.pepi.2006.07.008, 2006.

1384 Presti, D., Troise, C., and De Natale, G.: Probabilistic location of seismic sequences in heterogeneous media, Bull. Seismol.
1385 Soc. Am. 94, 2239-2253, DOI: 10.1785/0120030160, 2004.

1387 Presti, D., Orecchio, B., Falcone, G., and Neri, G.: Linear versus nonlinear earthquake location and seismogenic fault detection
1388 in the southern Tyrrhenian Sea. Italy, Geophys. J. Int. 172, 607-618, https://doi.org/10.1111/j.1365-246X.2007.03642.x, 2008.
1389

Robustelli, G., Russo Ermolli, E., Petrosino, P., Jicha, B., Sardella, R., and Donato, P.: Tectonic and climatic control on geomorphological and sedimentary evolution of the Mercure basin, southern Apennines, Italy, Geomorphology 214, 423-435, https://doi.org/10.1016/j.geomorph.2014.02.026, 2014.

Rovida, A., Locati, M., Camassi, R., Lolli, B., and Gasperini, P.: The Italian earthquake catalogue CPTI15, Bulletin of Earthquake Engineering, 18, 2953-2984, https://doi.org/10.1007/s10518-020-00818-y, 2020.

Rovida A., Locati M., Camassi R., Lolli B., Gasperini P., and Antonucci A.: Catalogo Parametrico dei Terremoti Italiani (CPTI15), versione 3.0. Istituto Nazionale di Geofisica e Vulcanologia (INGV). https://doi.org/10.13127/CPTI/CPTI15.3, 2021.

SCEC, 2021 https://www.scec.org/research/cfm; last access: 19 April 2021.

Schiattarella, M., Torrente, M., and Russo, F.: Analisi strutturale ed osservazioni morfotettoniche nel bacino del Mercure (Confine calabro-lucano), Il Quaternario, 7, 613-626, 1994.

Scognamiglio, L., Tinti, E., and Quintiliani, M.: Time Domain Moment Tensor (TDMT) [Data set]. Istituto Nazionale di Geofisica e Vulcanologia (INGV). https://doi.org/10.13127/TDMT, 2006.

Servizio Geologico d'Italia: 220 Verbicaro ~~Sheet~~ sheet of the Carta Geologica D'Italia, 1. 100.000 Scale. Rome, 1970.

Sgambato, C., Walker, J. P. F., and Roberts, G. P.: Uncertainty in strain-rate from field measurements of the geometry, rates and kinematics of active normal faults: implications for seismic hazard assessment, J. Struct. Geol 131, 103934.doi:10.1016/j.jsg.2019.103934, 2020.

Sketsiou, P., De Siena, L., Gabrielli, S., and Napolitano, F.: 3-D attenuation image of fluid storage and tectonic interactions across the Pollino fault network, Geophysical Journal International, 226(1), 536–547, https://doi.org/10.1093/gji/ggab109, 2021.

Sperner, B., Müller, B., Heidbach, O., Delvaux, D., Reinecker, J., and Fuchs, K.: Tectonic stress in the Earth's crust: advances in the World Stress Map project. In: New Insights into Structural Interpretation and Modelling (D.A. Nieuwland, ed.), J. Geol. Soc. London Spec. Publ., 212, 101–116, https://doi.org/10.1144/GSL.SP.2003.212.01.07, 2003.

Spina, V., Galli, P., Tondi, E., and Mazzoli, S.: Fault propagation in a seismic gap area (northern Calabria, Italy): implications for seismic hazard, Tectonophysics, 476, 357-369, https://doi.org/10.1016/j.tecto.2009.02.001, 2009.

Stirling, M., Goded, T., Berryman, K. and Litchfield, N.: Selection of Earthquake Scaling Relationships for Seismic-Hazard Analysis, Bulletin of the Seismological Society of America, 103(6), 2993-3011. https://doi.org/10.1785/0120130052, 2013.

Tangari, A.C., Scarciglia, F., Piluso, E., Marinangeli, L., and Pompilio, L.: Role of weathering of pillow basalt, pyroclastic input and geomorphic processes on the genesis of the Monte Cerviero upland soils (Calabria, Italy), Catena, 171, 299-315, ISSN 0341-8162, https://doi.org/10.1016/j.catena.2018.07.015, 2018.

Tarquini, S., Vinci, S., Favalli, M., Doumaz, F., Fornaciai, A., and Nannipieri, L.: Release of a 10-m-resolution DEM for the Italian territory: Comparison with global-coverage DEMs and anaglyph-mode exploration via the web, Computers and Geosciences, 38, 168-170. https://doi.org/10.1016/j.cageo.2011.04.018, 2012.

TDMT database – INGV http://cnt.rm.ingv.it/tdmt. last access: 19 April 2021.

Tertulliani, A., and Cucci, L.: New insights on the strongest historical earthquake in the Pollino region (southern Italy), Seismol. Res. Lett., 85(3), 743-751, https://doi.org/10.1785/0220130217, 2014.

Totaro, C., Presti, D., Billi, A., Gervasi, A., Orecchio, B., Guerra, I., and Neri, G.: The ongoing seismic sequence at the Pollino Mountains, Italy. Seismol. Res. Let., 84(6), 955-962, https://doi.org/10.1785/0220120194, 2013.

Totaro, C., Koulakov, I., Orecchio, B., and Presti, D.: Detailed crustal structure in the area of the southern Apennines–Calabrian Arc border from local earthquake tomography, J. Geodyn., 82, 87-97, https://doi.org/10.1016/j.jog.2014.07.004, 2014.

Totaro, C., Seeber, L., Waldhauser, F., Steckler, M., Gervasi, A., Guerra, I., Orecchio, B., and Presti, D.: An intense earthquake swarm in the southernmost Apennines: fault architecture from high-resolution hypocenters and focal mechanisms, Bull. Seismol. Soc. Am. 105, 1-6. https://doi.org/10.1785/0120150074, 2015.

Totaro, C., Orecchio, B., Presti, D., Scolaro, S., and Neri G.: Seismogenic stress field estimation in the Calabrian Arc region (south Italy) from a Bayesian approach, Geophys. Res. Lett., 43, 8960–8969, https://doi.org/10.1002/2016GL070107, 2016.

1455 Valoroso, L., Chiaraluce, L., Di Stefano, R., and Monachesi, G.: Mixed-Mode Slip Behavior of the Altotiberina Low-Angle
1456 Normal Fault System (Northern Apennines, Italy) through High-Resolution Earthquake Locations and Repeating Events, J.
1457 Geoph. Res. Solid Earth, 122(12), 10220-10240, https://doi.org/10.1002/2017JB014607, 2017.

1459 Van Dijk, J.P., Bello, M., Brancaleoni, G.P., Cantarella, G., Costa, V., Frixa, A., Golfetto, F., Merlini, S., Riva, M., Toricelli,
1460 S., Toscano, C., and Zerilli, A.: A regional structural model for the northern sector of the Calabrian Arc (southern Italy),
1461 Tectonophysics 324, 267-320, https://doi.org/10.1016/S0040-1951(00)00139-6, 2000.

1463 Vezzani, L., Festa, A., and Ghisetti, F.C.: Geology and tectonic evolution of the Central-Southern Apennines, Italy, Special
1464 Paper of the Geological Society of America, 469, 1-58, https://doi.org/10.1130/SPE469, 2010.

1466 Villani, F., and Pierdominici, S.: Late Quaternary tectonics of the Vallo di Diano basin (southern Apennines, Italy), Quat. Sci.
1467 Rev., 29, 3167-3183. https://doi.org/10.1016/j.quascirev.2010.07.003, 2010

1469 Waldhauser F., and Ellsworth W.: A Double-Difference Earthquake Location Algorithm: Method and Application to the
1470 Northern Hayward Fault, California, Bull. Seism. Soc. Am. 90(6):1353-1368, http://dx.doi.org/10.1785/0120000006, 2000.

1472 Waldhauser, F.: HypoDD: a Computer Program to Compute Double Difference Earthquake Locations. U.S. Geol. Surv, Menlo
1473 Park, California, pp. 01-113. Open-File Report, 2001.

1475 Wells, D.L., and Coppersmith, K.J.: New empirical relationships among magnitude, rupture length, rupture width, rupture
1476 area, and surface displacement, Bull. Seismol. Soc. Am., 84(4), 974-1002, 1994.

1478 Wesnousky, S.G.: Displacement and geometrical characteristics of earthquake surface ruptures: Issues and implications for
1479 seismic hazard analysis and the process of earthquake rupture, Bull. Seismol. Soc. Am., 98(4), 1609-1632.
1480 https://doi.org/10.1785/0120070111, 2008.

1482 Westoby, M.J., Brasington, J., Glasser, N.F., Hambrey, M.J., and Reynolds, J.M.: 'Structure-from-motion' photogrammetry:
1483 A low-cost, effective tool for geoscience applications, Geomorphology, 179, 300–314, 2012.